

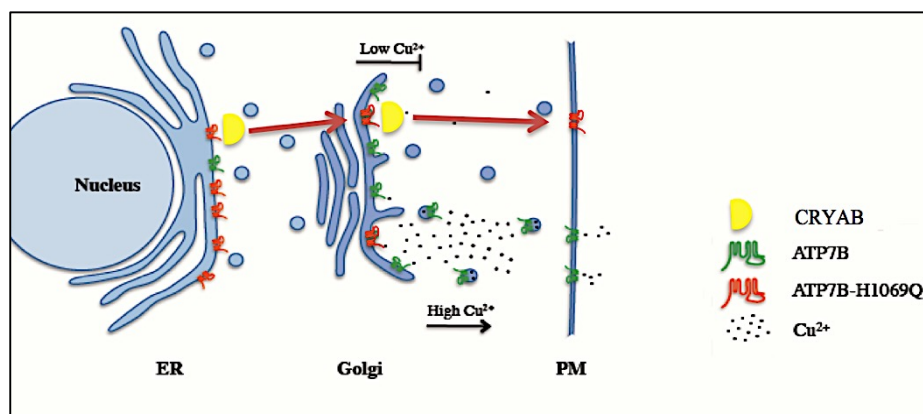
UNIVERSITY OF NAPLES FEDERICO II

DOCTORATE  
MOLECULAR MEDICINE AND MEDICAL  
BIOTECHNOLOGY

XXX CYCLE

Michela Ciano

**Tackling the Most Frequent Wilson Disease-  
Causing ATP7B Mutation: Mechanism of Rescue  
by  $\alpha$ B-Crystallin and its Derived Peptide**



Academic Year 2017/2018

**UNIVERSITY OF NAPLES FEDERICO II**

**DOCTORATE  
MOLECULAR MEDICINE AND MEDICAL  
BIOTECHNOLOGY**

**XXX CYCLE**



**Tackling the Most Frequent Wilson Disease-  
Causing ATP7B Mutation: Mechanism of Rescue  
by  $\alpha$ B-Crystallin and its Derived Peptide**

Mentor  
Prof. Stefano Bonatti

Candidate  
Michela Ciano

COORDINATOR  
Prof. Vittorio Enrico  
Avvedimento

**Academic Year 2017/2018**



## INDEX:

<b>ABSTRACT</b>	1
Abbreviations	3
<b>1. INTRODUCTION</b>	4
1.1 – Copper homeostasis	4
1.2 – Copper-transporting ATPases ATP7A and ATP7B in human diseases	6
1.3 – Wilson Disease (WD)	6
1.4 – Pathophysiology of the ATPase transporter ATP7B	10
1.5 – Small heat shock proteins	14
1.6 – $\alpha$ B-Crystallin (CryAB or HSPB5)	15
1.7 – $\alpha$ B-Crystallin-derived peptides	20
<b>2. AIMS OF THE THESIS</b>	23
<b>3. MATERIALS AND METHODS</b>	25
<b>4. RESULTS</b>	34
4.1 – Generation of phosphomimic and phosphodeficient CryAB forms	34
4.2 – Mimicking phosphorylation of $\alpha$ B-CryAB affects its chaperone function	35
4.3 – Pseudo-phosphorylation reduces the oligomerization state of CryAB	40
4.4 – $\alpha$ -Crystallin Domain rescues Golgi localization of ATP7B-H1069Q mutant	42
4.5 – CryAB peptide does not affect cell viability	44
4.6 – Internalization of CryAB peptide	46
4.7 – Peptide localizes mainly in the cytosol of COS7 cells	47
4.8 – Pept1, but not Ctrl Pept, rescues the Golgi localization of ATP7B-H1069Q	48

4.9 – The Golgi-corrected ATP7B-H1069Q moves to post-Golgi vesicles in response to Cu overload in the presence of Pept1	51
4.10 – Pept1, but not Ctrl Pept, interacts with ATP7B WT and H1069Q	53
4.11 – Pept1 increases ATP7B-H1069Q half-life	55
4.12 – Generation of hepatic differentiation of WD and control hiPSCs	56
4.13 – ATP7B expression in HLCs from patient and control hiPSCs	57
<b>5. CONCLUSIONS AND DISCUSSION</b>	<b>59</b>
<b>6. ACKNOWLEDGEMENT</b>	<b>64</b>
<b>7. REFERENCES</b>	<b>65</b>
<b>8. LIST OF PUBLICATIONS</b>	<b>77</b>

## ABSTRACT

Mutations in copper (Cu) transporter ATP7B are the primary cause of Wilson Disease (WD). WD is an autosomal recessive disorder characterized by hepatic cirrhosis and neuronal degeneration due to a severe impairment in biliary Cu excretion. The defective gene in WD encodes ATP7B, a Cu-transporting protein primarily expressed in the liver. Generally, ATP7B senses and responds to intracellular Cu levels via trafficking from the trans-Golgi network (TGN) toward post late-endosome (LE)/lysosomal compartments and plasma membrane (PM) to eliminate excessive Cu from the cell via bile canaliculi. The most frequent ATP7B disease-associated mutation (H1069Q) results in aberrant protein products that are mis-targeted from the Golgi complex to the endoplasmic reticulum (ER). However, ATP7B-H1069Q maintains a residual Cu-translocating activity believed to be sufficient to rescue Cu homeostasis when the protein is targeted to TGN (Kaler SG. *et al.*, 2011).

My research project expands previous studies conducted in my laboratory showing that the cytosolic holdase  $\alpha$ B-Crystallin (CryAB or Hsp-B5) rescues the localization and trafficking response of ATP7B-H1069Q to Cu overload (D'Agostino M. *et al.*, 2013).

In brief, the project was divided into two lines of research performed in collaboration with another Ph.D student Simona Allocca.

In the first line of research, we studied the effects of phosphorylation on CryAB full length structure and function and how phosphorylation can influence CryAB chaperone activity on ATP7B mutant. Our results show that mimicking phosphorylation of serine 19 and 45, either singularly or in combination reduces CryAB chaperone function. By contrast, phosphorylation of serine 59 has no such effect and counteracts the inhibition caused by single phosphorylation at S19 and S45. In addition, we found that all phosphomimetic substitutions lead to the formation of small oligomeric complexes containing CryAB, thereby suggesting that the reduction of the oligomerization state of CryAB does not correlate with the inhibition of its chaperone activity (Ciano M. *et al.*, 2016).

In the second line of research, we verified the rescue ability of CryAB domains on ATP7B-H1069Q. To this aim, we dissected CryAB in its main domains: N-terminal,  $\alpha$ -crystallin, and C-terminal. Subsequently, we assayed them through immunofluorescence analysis in cells co-transfected with ATP7B-H1069Q. We found that the  $\alpha$ -crystallin domain is able to rescue the Golgi localization of the ATP7B-H1069Q mutant. Then, since several studies have shown that small CryAB derived peptides are able to

mimic the effect of the full length protein, (Sreekumar P.G. *et al.*, 2013; Nahomi R.B. *et al.*, 2015), we focused on peptide 73-92, derived from the crystallin-domain of CryAB (Peptide1 or Pept1) in our WD cellular model. Our results revealed that Peptide1 retains the ability to rescue the Golgi localization of ATP7B-H1069Q, thereby fully mimicking the effects of the isolated  $\alpha$ -crystallin domain and full-length CryAB. Furthermore, we observed that Peptide1 and Control Peptide (Ctrl Pept) are taken up by COS7 and do not affect cell viability. Interestingly, we also demonstrated that Pept1, but not Ctrl Pept, is able not only to interact with ATP7B WT and H1069Q, but also to correct the localization of ATP7B-H1069Q from the ER to the TGN and to the post-TGN trafficking in response to toxic Cu. Moreover, our experiments revealed that Pept1 is also able to stabilize ATP7B-H1069Q, thereby increasing its half-life.

Finally, in collaboration with Dr. Silvia Parisi, Anna Musto, Simona Allocca, and Prof. Roman Polishchuk, we generated an isogenic cell model from iPSCs obtained from skin fibroblasts of a WD patient carrying the H1069Q mutation (H1069Q/H1069Q) and a familiar control (WT/H1069Q), and differentiated them into hepatocyte-like cells HLCs. Therefore, our future objective is to exploit these cells to study the expression, localization, mobilization, and function of the mutant ATP7B-H1069Q, and to test the rescue efficiency of peptide CryAB 73-92 (Peptide1).

## Abbreviations:

AAT,  $\alpha$ 1-antitrypsin;  
ACD,  $\alpha$ -crystallin domain;  
AFP,  $\alpha$ fetoprotein;  
ALB, albumin;  
Chx, Cycloheximide;  
CP, ceruloplasmin;  
CryAB or HSPB5,  $\alpha$ B-crystallin;  
CTE, C-terminal extension;  
CTR1, copper transporter 1;  
Ctrl Pept, control peptide;  
Cu, copper;  
ER, endoplasmic reticulum;  
ERK, p44/42 MAPK, p44/42 mitogen-activated protein kinase;  
FLIM, Fluorescence-lifetime imaging microscopy;  
HLCs, Hepatocyte-like cells;  
HSPs, Heat Shock Proteins;  
iPSCs, induced pluripotent stem cells;  
MBDs, metal binding domains;  
MD, Menkes Disease;  
MTT, 3-(4, 5-dimethylthiazolyl-2)-2, 5-diphenyltetrazolium bromide;  
N-terminal domain, NTD;  
p38, MAPK14, mitogen-activated protein kinase 14;  
Pept1,  $\alpha$ B-crystallin-derived peptide or peptide1;  
Pept2, control peptide or peptide2;  
Pept3, control peptide or peptide3;  
PM, Plasma Membrane;  
sHSPs, small Heat Shock Proteins;  
TAMRA, Tetramethylrhodamine;  
TGN, Trans Golgi Network;  
TMP, multispan transmembrane protein;  
UPR, unfolded protein response;  
WD, Wilson Disease.

## 1. INTRODUCTION

### 1.1 Copper homeostasis

Copper (Cu) is an essential micronutrient that plays a fundamental role in human metabolism. It is an important cofactor for many proteins and enzymes including superoxide dismutase 1 (Cu/Zn-SOD), cytochrome c oxidase (COX), lysyl oxidase, tyrosinase, dopamine- $\beta$ -hydroxylase, and ceruloplasmin (CP) (Arredondo M. and Núñez MT. 2005; de Bie P. *et al.*, 2007), which are involved in respiration, free radical scavenging, pigmentation, iron metabolism, collagen synthesis, elastin, and neurotransmitters.

For proper cellular function, the body needs to uptake an average of 1-3 mg of Cu daily. (Lutsenko S. *et al.*, 2007; Lutsenko S. *et al.*, 2010; Nevitt T. *et al.*, 2012). Indeed, when concentrations exceed the body's needs, Cu induces cellular toxicity because of its chemical redox potential. Accordingly, the amount of Cu in the body is carefully regulated. The main biochemical regulators of cellular copper metabolism are the Cu-transporting ATPases (Cu-ATPases) ATP7A and ATP7B. Mutations in ATP7A or ATP7B are associated with severe metabolic disorders, as they disrupt Cu homeostasis. In particular, disturbances in ATP7A result in Cu deficiency (Menkes disease, MD), whereas those in ATP7B give rise to Cu overload (Wilson disease, WD) (de Bie *et al.*, 2007).

Most of Cu absorption takes place in the duodenum. In brief, dietary Cu is taken up by enterocytes and is then delivered to the liver through the portal vein. This step is however blocked in MD (blue bars in Fig 1). After entering hepatocytes, Cu is distributed to other tissues through the general circulation. The great majority of Cu excretion from the body (98%) is performed by biliary export, suggesting that the liver constitutes the central organ of Cu homeostasis. In WD, Cu excretion from the liver is defective (red bars in Fig. 1), causing excess Cu overload in the liver (de Bie P. *et al.*, 2007). Under physiological conditions, Cu uptake in cells occurs through the Cu transporter 1 (CTR1) and is subsequently distributed by the Cu chaperone ATOX1 to ATP7A or ATP7B, residing in the trans-Golgi network (TGN) of enterocytes and hepatocytes, respectively. Increased levels of Cu prompt ATP7A and ATP7B to move from the TGN to the plasma membrane (PM) to facilitate Cu excretion. Therefore, ATP7A and ATP7B play a crucial role in excreting Cu from cells (de Bie P. *et al.*, 2007).

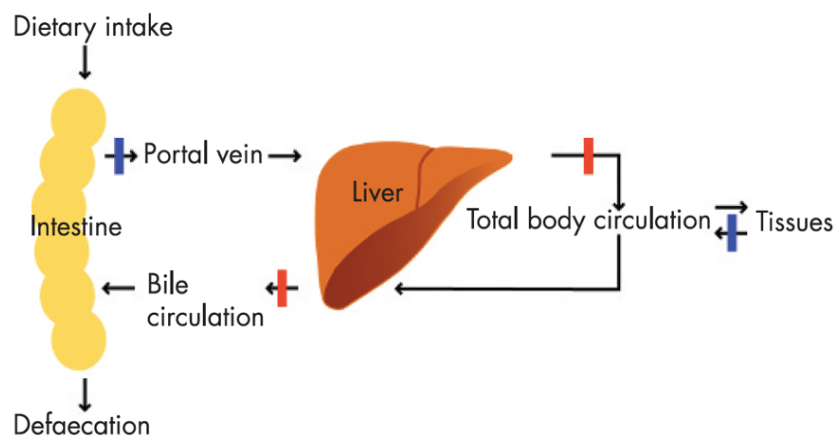


Figure 1. Schematic representation of Cu homeostasis (de Bie P. et al., 2007).

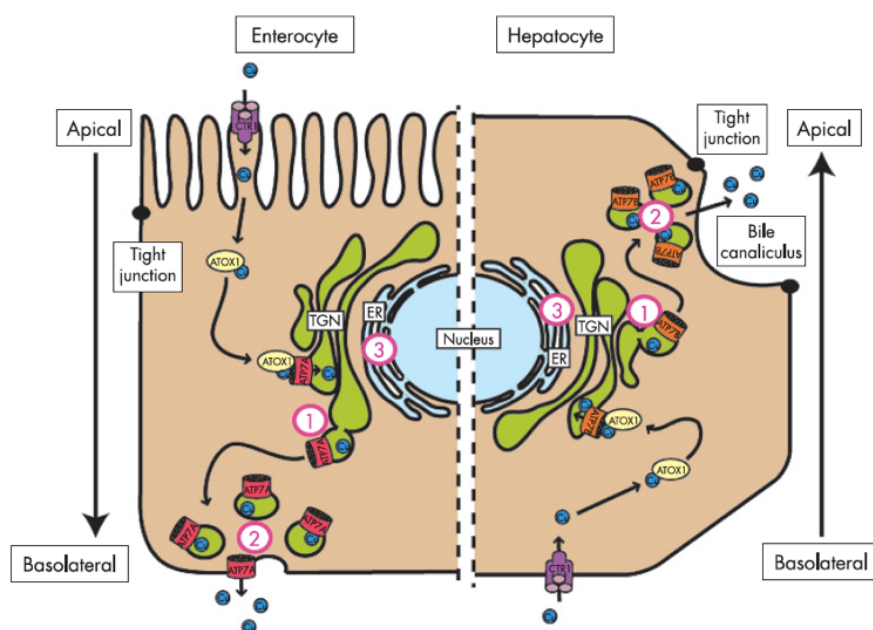


Figure 2. Schematic illustration of Cu-dependent localization of ATP7A and ATP7B. In both cell, enterocyte (left side) and hepatocyte (right side), Cu enters through the Cu transporter 1 (CTR1), and is then distributed via the Cu chaperone ATOX1 to ATP7A or ATP7B residing in the TGN. After increases in Cu concentrations, ATP7A and ATP7B relocate from the TGN to the cell periphery to facilitate Cu excretion (de Bie P. et al., 2007).

## **1.2 Copper-transporting ATPases ATP7A and ATP7B in human diseases**

Cu-ATPases are essential for maintaining Cu balance in cells and tissues. These evolutionary conserved polytopic membrane proteins translocate Cu from the cytosol across cellular membranes by using ATP hydrolysis energy, thus reducing intracellular Cu concentrations. In addition to removing excess Cu from the cell, Cu-ATPases perform important biosynthetic functions by supplying Cu to Cu-dependent enzymes within the secretory pathway. The importance of Cu-ATPases in human physiology can be illustrated by inherited copper-transport diseases resulting from mutations in the genes encoding ATP7A and ATP7B (De Bie P. *et al.*, 2007; Lutsenko S. *et al.*, 2007).

Mutations in the gene encoding the Cu-ATPase ATP7A cause Menkes disease (MD), a fatal X-linked copper-deficiency disorder in infants. Under physiological conditions, ATP7A facilitates Cu export from the enterocytes into the blood at the basolateral side. In MD, ATP7A is inactivated, thereby severely impairing the cell's ability to excrete Cu into the bloodstream. As a result, the more Cu accumulates in intestinal epithelium cells, the less it is delivered to the bloodstream, resulting in restricted Cu supply to other tissues (Kodama H. *et al.*, 1999). Copper deficiency is characterized by neurodegeneration, growth failure, coarse hair, and connective tissue abnormalities (Kaler S.G. *et al.*, 2011). On the other hand, mutations in the gene encoding the Cu-ATPase ATP7B lead to Wilson disease (WD), an autosomal recessive genetic disorder. Unlike MD, this disease is caused by toxic accumulation of Cu mainly in the liver and brain with development of severe hepatic, neurological, and psychiatric symptoms (see below) (Lutsenko S. *et al.*, 2007).

### **1.3 Wilson Disease (WD)**

WD, an autosomal recessive inherited disorder of Cu metabolism, is characterized by pathological Cu accumulation predominantly in liver and brain, where it induces cellular damage. However, it can also affect other organ systems like the kidneys, cornea, heart, and pancreas.

WD is observed with a prevalence of approximately 1:30,000 with a heterozygous ATP7B mutation carrier frequency of 1:90. Although the usual age of onset ranges from 3 to 50 years of age, this disorder has been detected in children as young as 3 and in adults as old as 70 (Ferenci P. 2003).

This disorder is produced by mutational defects of a protein that facilitates hepatic Cu excretion. The defective gene in WD encodes ATP7B (chromosome 13q14.3), a Cu-transporting protein primarily expressed in the liver (van de Berghe PV *et al.*, 2009).

This disease may present a variety of clinical conditions: commonly, hepatic and/or neuropsychiatric disorders; rarely, renal, skeletal, or endocrine symptomatology. In particular, approximately 45% of all WD patients present with liver disease, 35% with neurological defects, and 10% with psychiatric disturbances. The remaining 10% of initial presentations include hemolytic anemia, cardiomyopathy, jaundice, and a number of other less common conditions, all of which resulting from copper-mediated tissue injury. The great majority of patients (90%) present with Kayser-Fleischer rings, a deposition of copper in Descemet's membrane visible as a gold-brown ring around the outer edge of the cornea (Fig. 3) (Roberts E.A. and Schilsky M.L. 2003; Gitlin J.D. 2003; Ferenci P. 2003; de bie P. *et al.*, 2007).

The diagnosis of WD is very challenging, as it is based on a combination of symptoms and on the results of clinical, biochemical, and genetic tests. The tests used to diagnose WD include the following:

- Biochemical liver tests: Serum aminotransferase activities are generally increased in WD patients.
- 24-hours urine Cu test: Basal 24-hours urinary copper excretion is commonly elevated in WD.
- Serum Cu: Total serum Cu is usually decreased in proportion to the reduced ceruloplasmin levels in the circulation. However, in acute liver failure, it may be elevated because of the sudden release of Cu from liver tissue damage.
- Serum ceruloplasmin test: The serum ceruloplasmin is usually decreased in WD patients.
- Ophthalmologic slit lamp examination for Kayser-Fleischer (KF) rings.
- Liver biopsy for histology and histochemistry and Cu quantification.
- Neuroimaging: MRIs of the brain or CAT scans may detect structural abnormalities.
- Genetic testing for ATP7B mutations: A blood test identifies the genetic mutations that cause Wilson disease (Fig. 4) (Roberts E.A. and Schilsky M.L. 2003).

It is important to diagnose WD as early as possible since severe liver damage can occur before any signs of the disease begin to appear. Fortunately, if diagnosed and treated early enough, WD patients can live longer lives and enjoy a good quality of life.

Wilson disease treatment is based on two different approaches: (1) prompting Cu excretion from the body, (2) reducing dietary Cu absorption. The first approach is achieved by Cu chelation agents like D-penicillamine, trientine, or ammonium tetrathiomolybdate (TTM). Pharmacodynamically speaking, D-penicillamine binds Cu and enables patients to excrete excess Cu accumulated in the liver through their urine. Similarly, trientine gives the same results as D-penicillamine, but with fewer side effects, which commonly include hypersensitivity reactions, bone marrow suppression, and autoimmune diseases.

The second approach is obtained by ingestion of zinc and a low Cu diet. More recently, experimental treatments with TTM have revealed promising results particularly because when taken with meals, it prevents dietary Cu absorption. Furthermore, TTM appears to be an excellent form of initial treatment in patients who have neurological symptoms. Dietary Cu absorption is effectively inhibited by zinc ingestion and by low Cu diet. Accordingly, physicians recommend avoiding certain types of foods including mushrooms, nuts, chocolate, dried fruits, liver and molluscs. In effect, zinc interferes with the uptake of Cu from the gastrointestinal tract, by inducing metallothionein production in enterocytes, a cysteine-rich protein that is an endogenous chelator of metals. Having a greater affinity for Cu than for zinc, it inhibits Cu entry into the portal circulation. Ultimately, once bound, Cu is no longer absorbed but is lost in the feces (Roberts E.A. and Schilsky M.L, 2008).

Today, the mainstay of treatment for WD remains lifelong zinc-based pharmacological therapy; however, if treatment is ineffective, or in circumstances of fulminant liver failure, liver transplantation provides an effective cure (Fig. 5) (Roberts E.A and Schilsky M.L 2003; de Bie P. *et al.*, 2007).

Hepatic	Asymptomatic hepatomegaly
	Isolated splenomegaly
	Persistently elevated serum aminotransferase activity (AST, ALT)
	Fatty liver
	Acute hepatitis
	Resembling autoimmune hepatitis
	Cirrhosis (compensated or decompensated)
Neurological	Fulminant hepatic failure
	Movement disorders (tremor, involuntary movements)
	Drooling, dysarthria
	Rigid dystonia
	Pseudobulbar palsy
	Seizures
	Migraine headaches
Psychiatric	Insomnia
	Depression
	Neuroses
	Personality changes
Other systems	Psychosis
	Renal abnormalities: aminoaciduria and nephrolithiasis
	Skeletal abnormalities: premature osteoporosis and arthritis
	Cardiomyopathy, dysrhythmias
	Pancreatitis
	Hypoparathyroidism
	Menstrual irregularities; infertility, repeated miscarriages

Figure 3. Clinical Patterns of Hepatic, Neurological, and Psychiatric Disorders in WD patients (Roberts E.A and Schilsky M.L 2003).

TEST	COMMENTS
Biochemical indices	Abnormal liver function test (ALT, AST, ALP)
Urinary Copper	24 hours copper excretion >100µg in 65% of WD patients
Serum copper	Serum copper may be low in asymptomatic cases (because ceruloplasmin is low) or high in cases with active liver disease (because copper is raised)
Serum Ceruloplasmin	<20µg/dl (in 95% of WD patients)
KF rings	KF rings are present in only 50% to 62% of WD patients with mainly hepatic disease at the time of diagnosis
Liver Copper	>250µg/gm of dry weight liver
Coombs negative haemolytic anaemia	
Neuroimaging	Abnormal
Genetic testing	Over 200 mutations are known

Figure 4. Schematic illustration of the diagnostic criteria for WD.

Drug	Mode of Action	Neurologic Deterioration?	Side Effects	Comments
D-penicillamine	General chelator: induces cupriuria	10% to 50% during initial phase of treatment	Fever, rash, proteinuria, lupus-like reaction Aplastic anemia Leukopenia Thrombocytopenia Nephrotic syndrome Degenerative changes in skin Elastosis perforans serpiginosa Serous retinitis Hepatotoxicity	Reduce dose for surgery to promote wound healing and during pregnancy
Trientine	General chelator: induces cupriuria	Occasionally during initial phase of treatment	Gastritis Aplastic anemia rare Sideroblastic anemia	Reduce dose for surgery to promote wound healing and during pregnancy
Zinc	Metallothionein inducer: blocks intestinal absorption of copper	During initial phase of treatment	Gastritis; biochemical pancreatitis Zinc accumulation Possible changes in immune function	No dosage reduction for surgery or pregnancy
Tetrathiomolybdate	General chelator: blocks copper absorption, induces intestinal and urinary copper loss	Reports of only rare neurologic deterioration during initial treatment	Anemia; neutropenia	Experimental in the United States and Canada

**Figure 5. Pharmacological Treatment Modalities for WD** (Roberts E.A and Schilsky M.L. 2003).

#### 1.4 Pathophysiology of the ATPase transporter ATP7B

ATP7B, the Cu-ATPase transporter involved in WD, is a multispan transmembrane protein (TMP) composed of 1465 amino acids. It contains eight transmembrane helices, which form a channel that pumps Cu from the cytosol at the expense of ATP hydrolysis (Fig. 6).

The NH<sub>2</sub>-terminal portion of ATP7B is large (600 residues) and is composed of six metal binding domains (MBDs) that are connected by flexible loops. Each MBD binds one Cu and contains the repetitive sequence motif MxCxxC. Cu binds in the reduced Cu(I) form, and the two Cys residues in the metal-binding motif CxxC are the only Cu-coordinating ligands (Di Donato M. *et al.*, 2000; Wu F. *et al.*, 2015; Lutsenko S. *et al.*, 2007). *In vitro*, and perhaps *in vivo*, other metals such as zinc (Di Donato M. *et al.*, 2002) or lead (Qian Y. *et al.*, 2005) also bind to the NH<sub>2</sub>-terminal domain; however, the functional consequences and physiological significance of zinc or lead binding still remain unknown. The MxCxxC motifs are the site of Atox1 interaction and subsequent Cu binding (Wu F. *et al.*, 2015). Recent studies demonstrate that although mutation of all six NH<sub>2</sub>-terminal MBDs in ATP7B does not alter protein expression, it does disrupt ATP7B function (Cater M.A. *et al.*, 2004). The conserved Met, Leu, and Phe (Pro in MBD3) residues, spatially close to the CxxC motif, form a hydrophobic nucleus that probably establishes the metallic protein complex

(Lutsenko S. *et al.*, 2007).

The catalytic activity of ATP7B (the binding and hydrolysis of ATP) is mediated through the coordinated action of the A-domain and the ATP-binding domain. The latter consists of two domains: the phosphorylation domain (the P-domain) and the nucleotide-binding domain (the N-domain) (Efremov R.G. *et al.*, 2004).

The P-domain contains the highly conserved sequence motif DKTG, which is essential for enzyme phosphorylation. In turn, phosphorylation of aspartic acid residue (Asp) from the DKTG sequence is crucial for Cu transport. Acyl-phosphates are in effect the phosphorylated intermediates that determine protein conformational changes and Cu transport to the opposite side of the membrane (Miller J.V. *et al.*, 1996).

The N-domain is instead involved in nucleotide binding (ATP) and contributes to ATP coordination. This domain contains a highly conserved SEHPL sequence. The histidine residue in this motif is conserved in all known Cu-transporting ATPases and is the site of the most common mutation (H1069Q) in WD patients (Thomas G. R *et al.*, 1995).

The A-domain is the place where acyl-phosphates are dephosphorylated. This domain contains a Thr–Gly–Glu sequence motif (TGE) in which the Glu residue is crucial for phosphatase activity. Dephosphorylation of acyl-phosphates marks the completion of the cycle (Petris M.J. *et al.*, 2002).

The cytosolic C-terminal domain is relatively short (80–100 residues) and contains conserved trileucine motifs, which are required for retrieval of the transporter from the PM and vesicles (Mercer J.F. *et al.*, 2003; Petris M.J. *et al.*, 1998). Therefore, the C-terminal plays an important role in maintaining protein stability and in regulating protein location (Fig. 6) (Hsi G. *et al.*, 2004).

As for its function, ATP7B, which is localized in the TGN, receives dietary Cu from the cytosolic metallochaperone, Atox1. ATP7B then transfers Cu across the membrane into the lumen of the TGN. In hepatocytes, following transport into the lumen, Cu is incorporated into the Cu-dependent ferroxidase ceruloplasmin (CP), which is subsequently secreted into the blood. Excess cytosolic Cu induces ATP7B to move from the TGN to the endo-lysosomal organelles and to the PM of bile canaliculi to guarantee Cu excretion through the bile (Fig. 7) (Wu F. *et al.*, 2015).

More than 200 mutations WD gene have been reported to hamper the function of ATP7B. Mutations affect every position of the gene, including exons, introns and promoters. They have been classified as frameshift, nonsense, involved in splicing defects and missense mutations. The latter are the most common and are associated with a more severe WD phenotype (Gromadzka G. *et al.*, 2005) In particular, the most common missense

mutations are H1069Q (in Europe) and R778L (in Asia) (Ferenci P. 2004).

ATP7B-H1069Q is the most frequent WD-causing mutation among the Caucasian population (50%), where the histidine in position 1069 is substituted with a glutamine (de Bie P. *et al.*, 2007; Lutsenko S. *et al.*, 2007; Payne A.S. *et al.*, 1998). The mutation alters the structure of NBD (Dmitriev O.Y. *et al.*, 2011). In brief, the protein becomes thermally unstable and can no longer pass the quality control, thereby accumulating in the ER of hepatocytes. Consequently ATP7B-H1069Q, unlike wild-type ATP7B, fails to reach the Golgi complex and to move further towards LE/lysosomal compartments and the PM in response to Cu overload. Moreover, the H1069Q mutant has a decreased half-life compared with the wild-type ATP7B (Dmitriev O.Y. *et al.*, 2011) and is thus rapidly degraded. Recently, studies have shown that expression of this ATP7B mutant activates the p38 and JNK stress kinase pathways, which, in turn, lead to the enhanced arrest and degradation of the ATP7B-H1069Q in the ER. (Concilli M. *et al.*, 2016). Therefore, failure to pump excess Cu out of hepatocytes into the bile duct causes the toxic buildup of Cu in the liver of WD patients (Fig. 8) (de Bie P. *et al.*, 2007).

Although little is known regarding ATP7B oligomerization, studies show that the 3rd and 4th Cu-binding sites in the N-terminal domain of ATP7B can aggregate *in vitro* (Banci L. *et al.*, 2008). The hypothesis is that H1069Q mutation may weaken the interaction between the NBD and the N-terminal domain since several copies of the ATP7B mutant bind to each other through the 3rd and 4th Cu-binding sites in their N-terminal domains, thereby generating ATP7B-H1069Q aggregates. Intriguingly, although this mutation affects the NBD of the protein, it leaves a significant level of residual Cu transport activity ranging from 20 to 70% of wild-type ATP7B protein (van den Berghe V. E. *et al.*, 2009; Iida M. *et al.*, 1998; Huster D. *et al.*, 2012; Chandhok G. *et al.*, 2016). Noteworthy, even just a residual Cu-translocating activity is believed to be sufficient for the rescue of Cu homeostasis if an ATPase mutant can be targeted to the proper destination (Kaler SG. 2011). Therefore, correction of the trafficking and localization of ATP7B-H1069Q should allow a substantial recovery of normal Cu metabolism, benefitting the majority of WD patients. Most important different treatments such as incubation at low temperature (Payne AS. *et al.*, 1998) or with curcumine (van den Berghe V. E. *et al.*, 2009), or expression of CryAB (D'Agostino M. *et al.*, 2013), or inhibition of p38 and JNK kinase (Chesi G. *et al.*, 2016) have proven effective in rescuing localization and Cu response of the mutant. These findings show that once ATP7B-H1069Q moves beyond ER, it traffics similarly to wild type

ATP7B, thus suggesting interesting and promising new strategies to fight the disease (D'Agostino M. *et al.*, 2013; Chesi G. *et al.*, 2016).

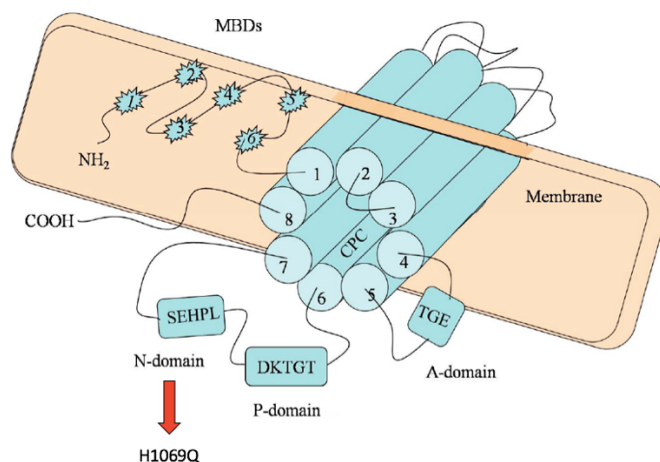


**Figure 6. Schematic structure of ATP7B.** ATP7B contains five regions: 1) an N-terminal tail with six metal-binding sites, 2) eight trans-membrane segments (TMS), 3) an ATP-binding domain that contains a nucleotide-binding motif (N-domain, SEHPL), and a phosphorylation motif (P-domain, DKTGT), 4) an A domain (TGE motif), and 5) a C-terminal tail. The H1069Q mutation occurs in the N domain (Wu F. *et al.*, 2015).

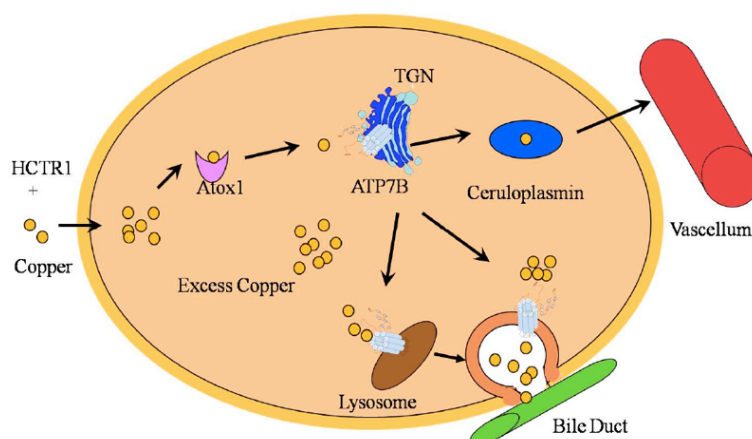


**Figure 7. Schematic illustration of Cu transport and metabolism in the liver.** Cu is delivered by the high-affinity Cu transport protein HCTR1 to the cytosol where it mainly binds to the metallochaperone, Atox1, which in turn transfers Cu to ATP7B located in the TGN. In the lumen of TGN, Cu is incorporated mostly into ceruloplasmin, which is released into the blood. Cu excess induces ATP7B to move from TGN to cytosolic vesicles to excrete Cu into the bile duct (De Bie P. *et al.*, 2007).

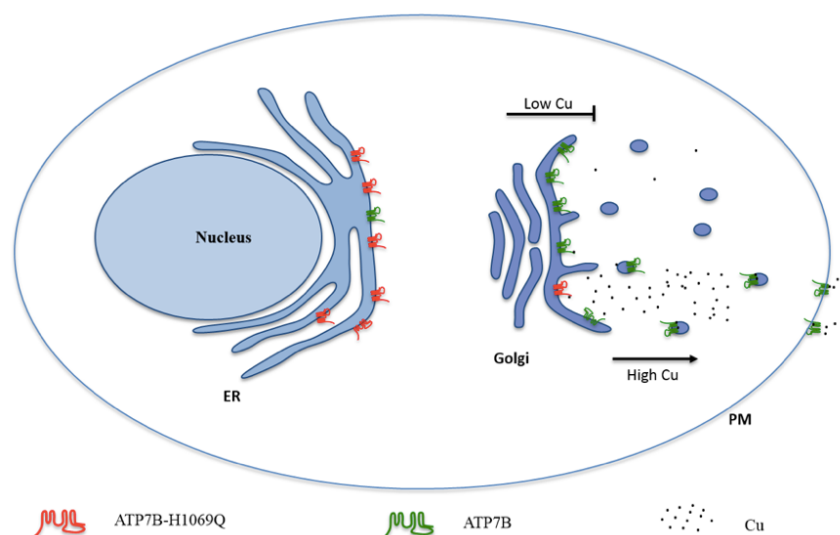


**Figure 8. Intracellular trafficking of ATP7B and ATP7B-H1069Q in the presence of low or high Cu concentration.** Under normal Cu levels, ATP7B resides into the TGN. In response to copper overload, ATP7B moves to the cytosolic vesicles and to the PM to excrete excess Cu into the bile canaliculi. ATP7B-H1069Q does not reach the Golgi, remaining mainly into ER as misfolded aggregates.

### 1.5 Small heat shock proteins

Unlike large heat shock proteins (HSPs) like HSP70 or HSP90, small heat shock proteins (sHSPs), hereafter called chaperones, are essential ‘holdase’ chaperones and cannot refold proteins (Narberhaus F. 2002). However, they sequester aberrant proteins to prevent subsequent formation of aggregates through an ATP-independent holdase activity. Subsequently, bound proteins can be transferred to ATP-dependent chaperones, such as Hsp70. Thanks to Hsp70, refolded and irreversibly damaged proteins are targeted to the ubiquitin-proteasome system (UPS) for degradation (Haslbeck M. and Buchner J. 2002).

sHSPs form large oligomers comprising up to 50 subunits and respond to stress conditions (pH, temperature, reduction and oxidation) to protect target proteins from aggregation and precipitation. They are ubiquitous intracellular proteins characterized by a highly conserved crystallin-core domain containing 80-100 amino acid residues (Nahomi R.B. *et al.*, 2015). The human genome encodes 10 members of the sHSP family with a molecular mass in the range of 12-43 KDa (Rajagopal P. *et al.*, 2015;

Arrigo A.P. *et al.*, 2007). The major members of the sHsp family are Hsp20 (HspB6), Hsp27 (HspB1) and  $\alpha$ B-crystallin (Schwarz L. *et al.*, 2009).

Intriguingly, some sHsps show anti-apoptotic or anti-inflammatory effects and interact with cytoskeletal elements. In addition, these proteins are tumorigenic when expressed in cancer cells (Bartelt-Kirbach B. and Golenhofen N. 2013).

Therefore, sHSPs are also involved in physio-pathological conditions and human diseases such as neurodegenerative disorders, myopathies, asthma, cataracts and cancers (Arrigo AP. *et al.*, 2007).

### 1.6 $\alpha$ B-Crystallin (CryAB or HSPB5)

Crystallin proteins are the major components of the mammalian lens fiber cell. They are subdivided into three classes,  $\alpha$ ,  $\beta$ , and  $\gamma$ , which account for nearly 90% of the lens proteins.  $\alpha$ -Crystallin, a member of the sHSP family, is the predominant type (Bloemendal H. 1981). It exists as a large heterogeneous aggregate (~800 kDa) comprising two types of subunits,  $\alpha$ A (HspB4) and  $\alpha$ B (HspB5), in a 3:1 ratio *in vivo* with chaperone-like holdase function. Amino acid sequences of the two subunits share 55% homology with each other and with other sHSPs.

In particular,  $\alpha$ A-Crystallin is predominantly present in the lens, whereas  $\alpha$ B-crystallin – in addition to being localized in the lens – is also present in several other tissues, including the retina, skeletal muscles, heart, and kidney (Nahomi RB. *et al.*, 2013; Nagaraj RH. *et al.*, 2015). The other two crystallins,  $\beta$ - and  $\gamma$ -crystallin, have no chaperone activity and serve as structural proteins (Bloemendal H. *et al.*, 2004).

Besides its chaperone activity,  $\alpha$ B-Crystallin participates in many cellular functions. It inhibits several processes like protein aggregation, oxidative stress, apoptosis, and inflammation; moreover, it provides neuroprotection and promotes angiogenesis, apoptosis, proteosomal protein degradation, and autophagy (Fig. 9) (Kannan R. *et al.*, 2012). Regarding its angiogenic properties, studies show that it directly acts as a chaperone for VEGF and other growth factors such as fibroblast growth factor-2 (FGF-2) (Ghosh JC. *et al.*, 2007a).

As for its anti-apoptotic properties, several findings have revealed that, in different cell types,  $\alpha$ B-crystallin inhibits apoptosis in conditions of cellular stress induced by TNF $\alpha$ , UV light, high glucose, okadaic acid, and staurosporine. It inhibits apoptosis in both mitochondrial and death receptor-mediated pathways. Interestingly, several other studies have

shown that  $\alpha$ B-crystallin directly interacts with pro-apoptotic Bcl-2-related proteins and Caspase-3, thereby preventing Bax and Bcl-X<sub>S</sub> mitochondrial translocation and caspase activation. Further, the antiapoptotic function of  $\alpha$ B-crystallin is also due to activation of phosphatidylinositol-3-kinase (PI-3K), and inhibition of phosphatase and tensin homolog (PTEN).

In association with its anti-apoptotic properties,  $\alpha$ B-crystallin protects various cell types during oxidative stress by increasing the expression of antioxidants, such as glutathione. Furthermore, in response to TNF- $\alpha$  treatment,  $\alpha$ B-crystallin enhances phosphorylation and subsequent proteosomal degradation of I $\kappa$ B $\alpha$ , a crucial step in NF- $\kappa$ B activation (Adhikari AS. *et al.*, 2011). Moreover, CryAB participates in protein degradation pathways. In particular,  $\alpha$ B-Crystallin specifically interacts both *in vitro* and *in vivo* with C8/ $\alpha$ 7, one of the 14 subunits of the 20S proteasome (Boelens WC. *et al.*, 2001).

As for autophagy,  $\alpha$ B-crystallin is involved in chaperone-mediated autophagy (CMA). In particular, it acts by increasing degradation of misfolded proteins and aggregates (Kannan R. *et al.*, 2012).

Structurally,  $\alpha$ B-Crystallin (CryAB or HspB5) is a small cytosolic protein of 175 amino acids. As other sHSPs, it comprises a poorly conserved N-terminal domain, a highly conserved  $\alpha$ -Crystallin domain (ACD), and a short C-terminal extension (Fig. 10). The chaperone activity of CryAB is affected by post-translational modifications of the N-terminal domain such as phosphorylation, oxidation, deamidation, glycation, acetylation, and truncation.

Little is known about the effect of post-translational modifications on the CryAB chaperone activity and several studies provide conflicting conclusions. In fact, both the influence of these modifications and the structure-function relationship of CryAB are still controversial (Nagaraj R.H. *et al.*, 2015).

Phosphorylation is one of the most important post-translational modifications. Under conditions of different stresses (heat, ischemia, and hypoxia), CryAB is phosphorylated at three serine residues, *i.e.*, 19, 45, and 59, *in vivo*, (Fig 10) by different protein kinases: p44/42 MAP kinase (ERK) and P38 MAP Kinase (P38). These kinases target Ser-45 and Ser-59, respectively. However, the signaling pathway leading to phosphorylation of serine 19 is currently unknown (Fig 11) (Kannan R. *et al.*, 2012).

The influence of phosphorylation at these residues on the chaperone activity of CryAB is controversial. Several studies using phosphorylation mimics demonstrate increased phosphorylation leads to the formation of smaller oligomeric complexes (Ito H. *et al.*, 2001) and enhances chaperone

activity (Ecroyd H. *et al.*, 2007). In contrast, phosphorylation-dependent induction of small oligomeric structures reduces CryAB chaperone activity (Aquilina J.A. *et al.*, 2004).

Interestingly, studies in cardiomyocytes and cancer cells found that Ser-59 phosphorylation of CryAB contributes to maximal apoptosis prevention (Launay N. *et al.*, 2010; Morrison L.E. *et al.*, 2003). However, another study found that oxidative stress by TNF- $\alpha$  causes CryAB phosphorylation at Ser-59 and phosphorylated  $\alpha$ B-crystallin associates and increases the kinase activity of the IKK complex, thus facilitating phosphorylation and subsequent degradation of I $\kappa$ B (Adhikari A.S. *et al.*, 2011).

In addition to phosphorylation, CryAB also undergoes deamidation, which is one of the most frequent *in vivo* modifications during aging and cataract development. Deamination not only alters secondary and tertiary structures as well as oligomerization properties but also reduces the levels of chaperone activity. In particular, the deamidation of an Asn (N) residue at position 146 (N146) but not at position 78 (N78) has profound effects on the structural and functional properties of CryAB (Gupta R. and Srivastava O.P. 2004).

C-terminal truncation is another modification that decreases CryAB chaperone activity (Takeuchi N. *et al.*, 2004). However, this type of modification alters not only conformation and thermal stability, but also susceptibility to degradation by the ubiquitin-proteasome pathway (UPP) (Zhang X. *et al.*, 2007). For instance, diabetic lenses show enhanced C-terminal truncation, which could lead to increased protein aggregation, ultimately causing diabetic cataracts (Thampi P. *et al.*, 2002).

Glycation is another major modification of CryAB. Glycation by sugars and ascorbate reduces chaperone function, whereas glycation by methylglyoxal (MGO), a metabolic  $\alpha$ -dicarbonyl compound, enhances its chaperone function (Nagaraj R.H. *et al.*, 2003).

Acetylation of lysine residues is another important modification that increases chaperone activity. In particular, acetylation at K92 in  $\alpha$ B-crystallin increases both chaperone and anti-apoptotic activities (Nahomi R.B. *et al.*, 2013; Kannan R. *et al.*, 2012).

All these observations suggest a controversial effect of post-translational modifications on the structure and functions of  $\alpha$ -crystallin (Nagaraj R.H. *et al.*, 2015).

Several mutations have been associated with CryAB. The first, identified in 1998, is the R120G, a missense mutation associated with desmin-related myopathy and cataracts. In particular, it causes the loss of chaperone function and the formation of protein precipitates inside cells. There are

other mutations associated with many diseases, such as myopathy, neuropathy, ischemia, cataract, and cancer disorders in which the mutated form of CryAB fails to protect cells from abnormal protein aggregation (Vicart P. *et al.*, 1998).

A very recent study has intriguingly demonstrated that CryAB assists the folding of several multipass transmembrane proteins (TMPs) by interacting with their cytosolic face, thereby highlighting the positive function of this protein in some genetic diseases, like WD and Familial exudative vitreoretinopathy (FZ4-FEVR). In particular, in these two conditions, two mutated genes – i.e., ATP7B-H1069Q, a mutant form of the Cu transporter associated with WD and Frizzled4-L501fsX533, a frame-shift mutant associated with a rare form of FZ4-FEVR – accumulate in the ER and are not transported to their final destination (trans-Golgi network and plasma membrane, respectively). In the biomolecular scenario of WD, CryAB exerts its beneficial action by rescuing proper folding of ATP7B-H1069Q and by transporting it to the TGN and post-Golgi vesicles in response to Cu overload (Fig. 12) (D'Agostino M. *et al.*, 2103).

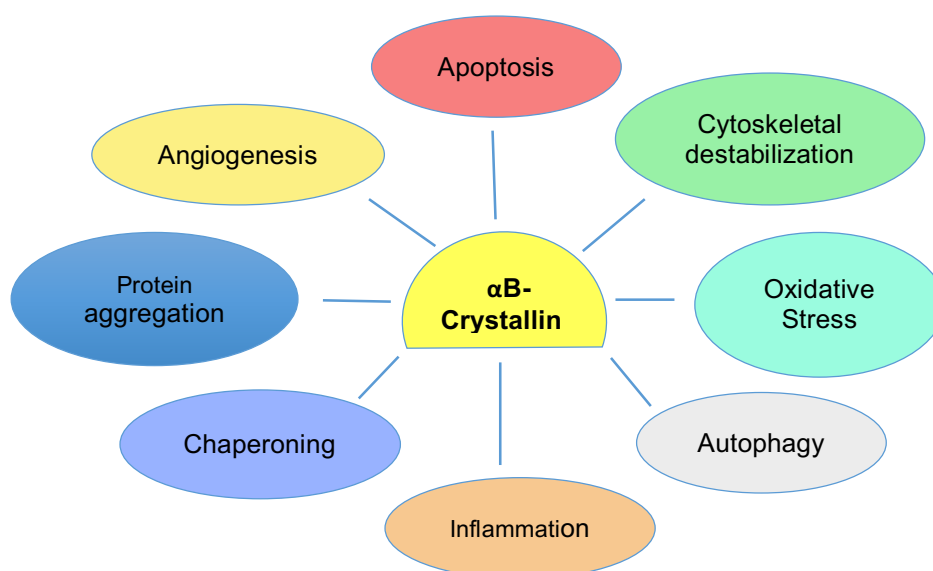


Figure 9. Schematic illustration of  $\alpha$ B-Crystallin cellular functions.

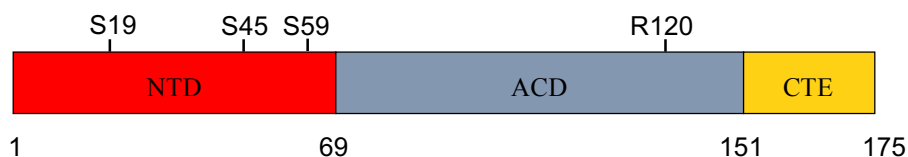


Figure 10. Schematic representation of 3 CRYAB domains and major phosphorylation in Serine residues (Ciano M. et al., 2016).

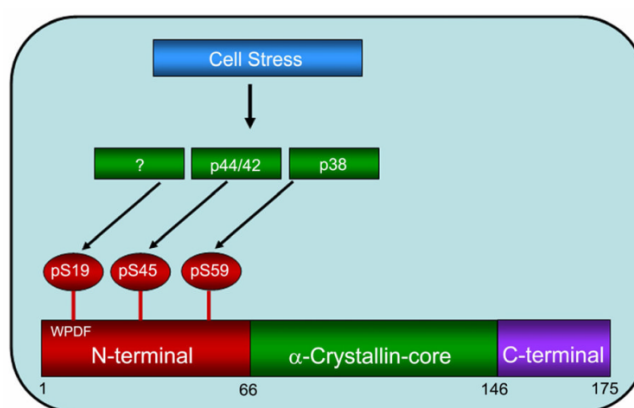


Figure 11. Structural organization of  $\alpha$ -crystallin protein.  $\alpha$ -Crystallins have a crystallin core domain flanked by variable NTD and CTE. Three known phosphorylation sites on  $\alpha$ B-crystallin are located in the NTD and can be activated by p44/42 and p38 MAP kinases, as well as by other still unknown pathways (Kannan R. et al., 2012).

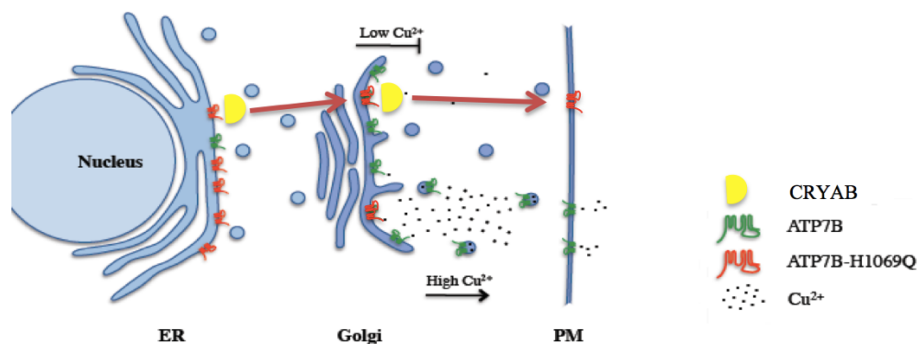


Figure 12. Rescue of localization and response to Cu overload of ATP7B-H1069Q by the cytosolic holdase CryAB. ATP7B-H1069Q, assisted by CryAB, folds into the proper conformation, moves to the Golgi complex, and responds to Cu overload similarly to wild-type ATP7B.

### 1.7 $\alpha$ B crystallin-derived peptides

Previous studies have demonstrated that CryAB acts like a molecular chaperone and forms a stable complex with partially unfolded proteins. Its chaperone activity depends on its binding affinity for target proteins (Horwitz J, 1992). Although the molecular mechanisms by which chaperones interact with unfolded proteins are still unclear, several studies determined the regions involved in its chaperone function. The regions that most likely interact with a number of target proteins have been identified with a variety of biochemical approaches *in vitro* (protein crosslinking methods). It has been hypothesized that the N-terminal phenylalanine-rich region (Plater M. L. *et al.*, 1996) and the hydrophobic sequences in the Crystallin domain, as in the case of the molecular chaperone GroEL, are responsible for chaperone-like activity. Another study on sHSP  $\alpha$ B-crystallin reports that residues 57–69 and 93–107 in  $\alpha$ B-crystallins are involved in chaperoning ADH (alcohol dehydrogenase) (Sharma KK. *et al.*, 1997; Sharma KK. *et al.*, 2000).

To determine which site of CryAB retains chaperonic functions, several peptides have been synthesized to study their functional activity. The synthetic peptides exhibiting chaperone activity have been called “mini-chaperones” or “mini- $\alpha$ B peptide” (Raju M. *et al.*, 2016). It has been shown that the isolated peptides corresponding to residues 73-85 and 101-110 of the crystallin domain have anti-fibril formation activity (Ghosh JG. *et al.*, 2008), whereas peptide 73-92 prevents aggregation and precipitation of unfolding proteins, similar to the full-length native  $\alpha$ -crystallin (Bhattacharyya J. *et al.*, 2006).

Ghosh and Clark identified additional chaperone peptides representing specific regions of CryAB:  ${}_{73}\text{DRFSVNLVDVKHFS}_{85}$ , (N terminal domain)  ${}_{113}\text{FISREFHR}_{120}$ , (N terminal domain)  ${}_{131}\text{LTITSSLSDGV}_{142}$  ( $\alpha$  crystallin core domain) and  ${}_{156}\text{ERTIPITRE}_{164}$  (C-terminal extension) (Ghosh JC. and Clark JI. 2005). All these peptides are endowed with chaperone activity against partially unfolded ADH. In addition, the minimal sequence of the peptide crucial for chaperone activity has been studied to develop effective and potent chaperone(s) for therapeutic purposes (cataract, neurodegenerative diseases and other protein aggregation disorders). However, none of these ‘modified’ peptides exhibit better chaperone function than the original mini- $\alpha$ B sequence 73-92. In contrast, deletion of DRFS residues from the N-terminal side (mini- $\alpha$ B 77-92) or deletion of LKVK from the C-terminal side (mini- $\alpha$ B73-88) of mini- $\alpha$ B completely impairs chaperone activity (Raju M. *et al.*, 2016). Other studies have demonstrated that the peptide  ${}_{70}\text{KVFIFLDVKHFSPEDLTVK}_{88}$  in  $\alpha$ A-

crystallin and the peptide  ${}_{73}\text{DRFSVNLDVKHFSPEELKVK}_{92}$  in  $\alpha\text{B}$ -crystallin act as mini-chaperones inhibiting stress-induced aggregation of several proteins similar to the parent molecules. In particular, they prevent stress-induced apoptosis in mammalian cells by blocking cytochrome c release from mitochondria and the caspase-3 and -9 activity. In organ-cultured rat lenses, the peptides inhibit calcimycin-induced epithelial cell apoptosis, whereas intraperitoneal injection of the peptides inhibit cataract development in selenite-treated rats, which is accompanied by inhibition of protein insolubilization, oxidative stress, and caspase activity in the lens (Nahomi RB. *et al.*, 2013).

Similar results have been obtained with peptides in heat-shock protein Hsp20 (G71HFSVLLDVKHFSPEEIAVK91) and Hsp27 (D93RWRVSLDVNHFAPELTVK113), with sequence homology to  $\alpha\text{B}$ -crystallin. Both peptides exhibit robust chaperone and anti-apoptotic activities and inhibit hyperthermic and chemically induced aggregation of client proteins. Thus, they may have therapeutic benefits in diseases associated with protein aggregation and apoptosis. (Nahomi RB. *et al.*, 2015). In conclusion, data show that the 20mer peptide “DRFSVNLDVKHFSPEELKVK” is the top performing chaperone. This sequence, which is highly conserved across many small heat shock proteins corresponds to the amino acids 73–92.

Transport systems that mediate the uptake of oligopeptides have been known to exist in mammalian cells. In particular, the oligopeptide transporters SOPT1 and SOPT2 (sodium-coupled oligopeptide transport system 1 and 2) are the two putative transporters for  $\alpha$ -Crystallin peptides. Consistently, a recent study by Sreekumar *et al.*, has shown that the mini- $\alpha\text{B}$  73-92 peptide enters human fetal retinal pigment cells (hfRPE), via SOPT1 and SOPT2 and protects them from oxidative stress-induced apoptosis; however, a much better protection is provided by the uptake of peptide-containing nanoparticles into cells (Sreekumar PG. *et al.*, 2013).

On the basis of this insightful evidence, my research project set out to investigate whether the activity of the mini- $\alpha\text{B}$  73-92 in our WD cellular model might act as a chaperone for the folding, localization, and activity of ATP7B-H1069Q and work as efficiently as the full-length CryAB.

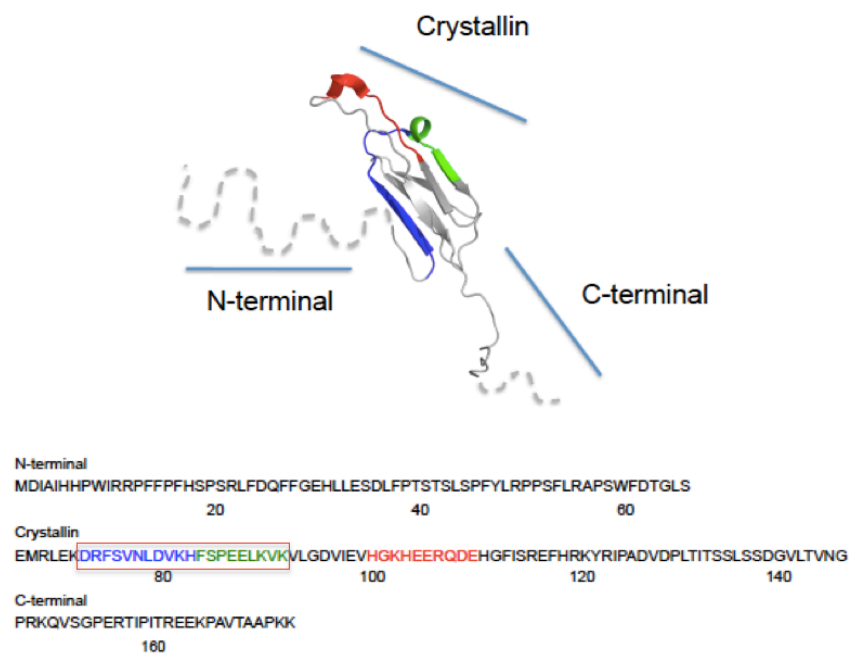


**Figure 13. Structural model and primary sequence of CryAB protein and its derived peptides.** Dashed line: region of the protein for which no crystallographic data are available. The N-terminal,  $\alpha$ -Crystallin, and C-terminal extension domains are indicated. In the crystallin domain, the three major peptides endowed of chaperone activity in vitro (73-85, 73-92 and 101-110) are indicated in blue, blue + green, and red, respectively. In the red square is indicated the peptide sequence (73-92) mentioned in this thesis.

## 2. AIMS OF THE THESIS

My project carried out in Professor Bonatti's laboratory, in collaboration with Simona Allocca, focused on the study of sHSPB5  $\alpha$ B-crystallin (CryAB). This sHSP is known for its chaperone activity on the mutated Cu transporter ATP7B-H1069Q, the most common cause of WD. Previous results obtained from our laboratory have demonstrated that CryAB acts as a holdase, thereby preventing improper aggregation and rescuing the Golgi complex localization of ATP7B-H1069Q (D'Agostino M. *et al.*, 2013). Studies show that this sHsp forms large and dynamic homo- and hetero-oligomeric complexes that are important in carrying out holdase chaperone activity (Arrigo A.P. *et al.*, 2007). However, as of today, the relationship between CryAB oligomer size, phosphorylation status, and chaperone activities is still controversial (Morrison L.E. *et al.*, 2003).

Recent studies show that CryAB peptides can also act as mini-chaperones *in vitro* and *in vivo*, thereby mimicking the effects of full-length protein (Sreekumar PG. *et al.*; Nahomi RB *et al.*, 2015). In effect, compared to native proteins, peptides may be more effective because they are smaller, may have greater specificity of action, and are more efficiently delivered to target tissues.

It is on the basis of this insightful evidence that my research project set out to investigate the activity of the synthetic peptide 73-92 derived from the crystallin-domain of CryAB (Peptide1) in our WD cellular model. Actually, the rationale behind the project was that this mini-chaperone could represent a new and interesting therapeutic alternative to the full-length protein in rescuing the proper intracellular localization of ATP7B-H1069Q. In this context, the aims of my project are focused on two lines of research.

The first is based on the study of the effects of phosphorylation on CryAB full-length structure and function and how phosphorylation can influence CryAB chaperone activity on ATP7B mutant. Previous findings have shown that phosphorylation of serine residues interferes with the degree of oligomerization and the activity of the chaperone (Ito H. *et al.*, 1997). Accordingly, we studied the effect of either the single pseudo-phosphorylated CryAB-S19D, -S45D and -S59D mutants or the double pseudo-phosphorylated mutants by using (1) immunofluorescence analysis (in cells co-transfected with ATP7B-H1069Q) to verify their rescue ability and (2) the glycerol gradient assay to study oligomerization.

The second line of research discussed in this thesis is based on CryAB dissection in its main domains: N-terminal,  $\alpha$ -crystallin, and C-terminal. In particular, we assayed each domain through immunofluorescence analysis in cells co-transfected with ATP7B-H1069Q to verify their rescue ability. Then, we tested the synthetic peptide 73-92 derived from the crystallin-domain of CryAB (Peptide1) in our WD cellular model. For this purpose, we performed MTT assays, cell growth curves, subcellular fractionation, coimmunoprecipitation and immunofluorescence analysis.

In addition, this thesis will discuss the generation of an isogenic cell model, based on iPSCs obtained from skin fibroblasts of a homozygous patient (H1069Q/H1069Q) and a familiar control (WT/H1069Q), followed by differentiation into HLCs. Remarkably, these cells represent a disease model that mimics much more closely a WD patient than the hepatoma cell lines currently used for transfection.

### 3. MATERIALS AND METHODS

#### *cDNA cloning and plasmid construction*

cDNA encoding CRYAB (ID: NM\_001885.1) cloned into pCMV6-XL5 vector plasmid was obtained from Origene. To obtain the construct 3xFLAG–CryAB, the cDNA coding for CryAB was amplified from pCMV6-XL5 plasmid by PCR using the following oligos containing HindIII/XbaI flanking restriction sites and cloned into p3xFLAG–CMV-7.1:

Fw (HindIII): 59-AAGCTTATGGACATCGCCATCCACCACCC-39;

Rv (XbaI): 59-TCTAGACTATTTCTTGGGGGCTGCGG-39.

To obtain the construct 3xFLAG–CryAB (R120G) in which the R120 was substituted with a glycine (G), the construct 3xFLAG–CryAB was used as a template and site direct mutagenesis was performed according to the manufacturer instructions (Roche) using the following oligos:

Fw: 59-CTCCAGGGAGTTCCACGGGAAATACCGGATCCCAG-39;

Rv: 59-GTGGAACTCCCTGGAGATGAAACC-39.

To obtain the construct HA-CryAB, the cDNA coding for CryAB was amplified from pCMV6-XL5 plasmid by PCR using the following oligos containing HindIII/XbaI flanking restriction sites and cloned into pCDNA3 expression vector (Invitrogen):

Fw (EcoRI): 59-GAATTCATGGACATCGCCATCCACCACCC-39;

Rv (XhoI): 59-CTCGAGCTATTTCTTGGGGGCTGCGG-39.

DNA of ATP7B and ATP7B-H1069Q GFP-tagged at the N-terminus was provided by Svetlana Lutsenko (John Hopkins Medical School, Baltimore, MD) and by Dominik Huster (Otto-von-Guericke-University, Magdeburg, Germany).

#### *Cloning strategy*

N-terminal (NTD),  $\alpha$ -crystallin (ACD) and C-terminal domains (CTE) were amplified using the Expand High Fidelity PCR System (Roche) and specific primers:

NTD: FW - 5'-GAATTCATGGACATCGCCATCCACC-3'

REV- 5'CTCGAGCTATGAGAGAGTCCAGTGTCAAACC-3'

ACD: FW - 5'-GAATTCCTCTCAGAGATGCGCCTGG-3

REV: 5'CTCGAGCTAATTCACAGTGAGGACCC-3'

CTE: FW: 5'-GAATTCCCAAGGAAACAGGTCTCTG-3'

REV: 5'-CTCGAGCTATTTCTTGGGGGCTGC-3'

The forward primers contain the restriction enzyme EcoRI recognition site, while the reverse primers contain the restriction enzyme XhoI recognition site. In the reverse primers used for the amplification of N-terminal and  $\alpha$ -crystallin domains is also present a stop codon. Restriction enzymes EcoRI and XhoI recognition sites are compatible with the multiple cloning sites on the HAN(I)-pcDNA3 expression vector. Amplified gene was cloned into pCR 2.1-TOPO cloning vector (Invitrogen) and transformed into TOP10 Escherichia coli (E. coli) cells. Transformed cells were selected on a LB plate containing 100  $\mu$ g/mL ampicillin at 37°C for 16-18 hours. Positive transformants were inoculated into LB broth containing 100  $\mu$ g/mL ampicillin for plasmid propagation. Plasmid was isolated and the presence of the DNA fragment of interest was determined by restriction enzyme digestion and DNA sequencing. The TOPO vector containing the DNA fragment of interest and the expression vector were then digested with the same enzymes (EcoRI and XhoI) to generate the same sticky ends. The digestion products of both the DNA fragment of interest and the expression vector were ligated at room temperature for 5 minutes using the Rapid DNA Ligation Kit (Roche). Ligated mixture was transformed into TOP10 E. coli cells and selected using the same strategies as described above.

### ***Cell culture***

Cells were maintained in 5% CO<sub>2</sub> at 37°C in a humidified chamber. The COS7 (monkey kidney fibroblast-like cells) cell line was grown in Dulbecco's modified essential medium (DMEM), supplemented with 10% of fetal bovine serum (FBS), 1% L-Glutamine and 1% Penicillin/Streptomycin. HepG2 (human hepatocellular carcinoma) cell line knockout for the expression of ATP7B (HepG2 KO), kindly provided by Roman Polishchuk, was routinely grown in Roswell Park Memorial Institute (RPMI) medium, containing 10% fetal bovine serum (FBS), 1%

L-Glutamine and 1% Penicillin/Streptomycin. ATP7B knockout was obtained by highly specific ZFN directed mutagenesis (Porteus MH. and Carroll D. 2005; Chandhok G. *et al.*, 2014). Huh7 (human hepatocellular carcinoma) cell line was grown in Dulbecco's modified essential medium (DMEM), supplemented with 10% of fetal bovine serum (FBS), 1% L-Glutamine and 1% Penicillin/Streptomycin.

### ***Transfection***

COS7, Huh7, or HepG2 KO cells were cultured on a coverslip in 24 well plates and after 24 hours were transfected with X-tremeGene HP Transfection Reagent (Roche) and JetPEI-Hepatocyte DNA Transfection Reagent (Polyplus transfection), respectively, according to the manufacturer's instructions.

### ***Viral transduction***

HepG2 KO cells were cultured on a coverslip in 24 well plates and after 24 hours were infected with an adenovirus carrying GFP-ATP7B-H1069Q. Human adenovirus type 5 (dE1/E3) was produced by Vector Biolabs in HEK 293 as packaging cells and CMV promoter drives the expression of GFP-ATP7B-H1069Q.

### ***Peptide treatment***

Peptide1 (H-Asp-Arg-Phe-Ser-Val-Asn-Leu-Asp-Val-Lys-His-Phe-Ser-Pro-Glu-Glu-Leu-Lys-Val-Lys-OH), Peptide2 or Ctrl Peptide (H-Lys-Val-Lys-Leu-Glu-Glu-Pro-Ser-Phe-His-Lys-Val-Asp-Leu-Asn-Val-Ser-Phe-Arg-Asp-OH), and Peptide3 or Ctrl Pept (H-Asp-Leu-Pro-Leu-Lys-Val-Asn-Val-Glu-Asp-Lys-Phe-His-Arg-Ser-Phe-Val-Glu-Ser-Lys-OH) were chemically synthesized by GL Biochem (Shanghai, China) and were then resuspended in H<sub>2</sub>O to obtain a final concentration of 5 mM. Synthetic peptides were labeled or not with TAMRA at the side chain amino group of Lysine residue at the Carboxy (Peptide1 and Peptide3)) and Amino terminal ends (Peptide2). All the peptides, resuspended in sterile H<sub>2</sub>O (25%) and RPMI or DMEM (75%), were added in the cell culture medium at a final concentration of 12,5 μM for 24 hours.

### ***Copper treatment***

COS7 cells, seeded on coverslips in 24 well plates, were transfected with pEGFP-C1-ATP7B WT or pEGFP-C1-ATP7B-H1069Q and treated with Pept1 or Ctrl Pept, as mentioned above. After 48 hours, 200  $\mu$ M of CuSO<sub>4</sub> or 500  $\mu$ M of BCS, was added to the cell culture medium for 2 hours. Then, the cells were subjected to indirect immunofluorescence procedure as below. Single confocal images were acquired at 63X magnification on a LSM510 Meta confocal microscope (Carl Zeiss, Jena, Germany).

### ***Immunofluorescence analysis***

COS7 or Huh7 cells were fixed in formaldehyde 3.7% for 30 minutes, washed with PBS 1X, and permeabilized with 0.1% Triton in PBS 1X. Non-specific signals were blocked in 1% BSA in PBS 1X for 15 minutes. The cells were then incubated for 1 hour with the following primary antibodies: anti-GOLGA2 (rabbit polyclonal, Sigma Aldrich) or anti-TGN46 (rabbit polyclonal, Sigma Aldrich) to visualize Golgi complex, anti-Lamp1 (mouse monoclonal, DSHB) to visualize lysosomes, and anti-Flag (mouse monoclonal, Sigma Aldrich) or anti-HA (mouse monoclonal, Sigma Aldrich). Next cells were washed three times in PBS 1X and incubated with Alexa Fluor 546-labelled anti-mouse and Alexa Fluor 633-labelled anti-rabbit secondary antibodies (Thermo Fisher) at room temperature for 45 minutes. Finally, nuclei were stained with Dapi (Sigma Aldrich). Single confocal images were acquired at 63X magnification on a LSM510 Meta confocal microscope (Carl Zeiss, Jena, Germany).

### ***MTT assay***

COS7 or HepG2 KO cells were plated in 96-well plates and, after 24 hours, exposed to 12.5  $\mu$ M of Pept1 or Ctrl Pept. At the indicated time points, 10  $\mu$ l of 5 mg/ml MTT solution was added to each well for 4 h at 37°C. After removal of the medium, 100  $\mu$ l of isopropanol plus 0,1M HCl was added to each well to dissolve formazan crystals. The absorbance at 570 nm was determined with the SYNERGY H1 microplate reader (Bio-Tek Instruments, Inc, Winooski, VT, USA). Triplicate wells were assayed for each condition and the S.D. was determined.

### ***Cell-growth assay***

HepG2 KO cells were seeded in 24 well plates. After 24 hours, they were treated with Pept1 or Ctrl Pept. Cell counts were performed in a Burker chamber, after 24, 48, and 72 hours from the treatment. After 72 hours, cells were replated in 12 well plates and peptides were readministered. Cell count was performed 72 hours later.

### ***Differential centrifugation***

COS7 cells were plated in p60 dishes. One day after growth, cells at 80% confluence were treated with TAMRA-labeled Pept1 or Ctrl Pept. After 24 hours, the cells were resuspended in lysis buffer (10 mM Tris-HCl pH 7.4, 150 mM NaCl pH 8.0, 1 mM EDTA pH 8.0, protease inhibitors), incubated 30 minutes on ice, and then lysed by sonication. The samples were centrifuged at 16.000xg at 4°C for 30 minutes, the pellets resuspended in lysis buffer, and the supernatants centrifuged at 100.000xg at 4°C for 30 minutes. Finally, the pellets were resuspended in lysis buffer supplemented with 1% Triton. All the pellets and the supernatants obtained from the 100.000xg centrifugation were analyzed by spectrofluorimeter.

### ***Co-immunoprecipitation***

COS7 cells were cultured in P100 plates and, after 24 hours, were transfected with pEGFP-C1-ATP7B-H1069Q, using X-tremeGene HP (Roche, Milan, Italy), according to the manufacturer's instructions. The next day, they were treated with 12.5  $\mu$ M of TAMRA-labeled Pept1 or Ctrl Pept for 24 hours. Then, cells were lysed with 10 mM Tris-HCl pH 7.4, 150 mM NaCl, 1 mM EDTA pH 8.0, 1% Triton X-100 and 1X Protease inhibitors (Roche). Immunoprecipitation was performed by overnight incubation at 4°C with mouse monoclonal anti-GFP antibody (Invitrogen), followed by addition of Protein A- Sepharose beads (Roche). The immunoprecipitated samples were analyzed through Mass Spectrometry (MS) by Chiara D'Ambrosio in the laboratory of Professor Scaloni at ISPAAM, Naples.

### ***Mass spectrometry***

Proteins/peptides were extracted from the beads with an aqueous 5% formic acid solution. The supernatants were transferred onto Centricon devices (3 kDa cutoff) (Millipore) and filtered by centrifugation at 14.000 g for 30 min. Resulting samples were dried and vacuumed, and then analyzed with a nanoLC-ESI-Q-Orbitrap MS/MS system, consisting of an UltiMate 3000 HPLC RSLC nano system-Dionex coupled to a Q-Exactive<sup>Plus</sup> mass spectrometer through a Nanoflex ion source (Thermo Fisher Scientific).

Peptides were loaded on an Acclaim PepMap<sup>TM</sup> RSLC C18 column (150 mm × 75 µm ID, 2 µm - particles, 100 Å - pore size (Thermo Fisher Scientific), and eluted with a gradient of solvent B (19.92/80/0.08 v/v/v water/acetonitrile/formic acid) in solvent A (99.9/0.1 v/v water/formic acid) at a flow rate of 300 nL/min. The gradient of solvent B started at 3%, increased to 10% over 5 min, increased to 30% over 40 min, rose to 80% over 5 min, remained at this percentage for 14 min, and finally returned to 3% in 1 min, remaining so for 30 additional minutes. The mass spectrometer operated in Selected Ion Monitoring (SIM) mode setting  $m/z=560.69 \pm 0.6$  (charge 5+) with nominal resolution of 70000, automatic gain control target of 50000, and a maximum ion target of 100 ms, followed by MS/MS scans of the most abundant ion. MS/MS spectra were acquired in a scan  $m/z$  range 120-2000 using a normalized collision energy of 32%, an automatic gain control target of 200000, a maximum ion target of 100 ms, and a resolution of 17500. Two biological replicates were analyzed.

### ***Western blot analyses and Chx treatment of HepG2 KO and HLCs***

HepG2 KO cells were cultured in 6 well plates, infected with an adenovirus carrying GFP-ATP7B-H1069Q, and incubated with Pept1 or Ctrl Pept, as previously mentioned. Then, they were treated with or without 100µM of cycloheximide (Sigma) for 2 hours, and subsequently lysed with 10 mM Tris-HCl pH 7.4, 150 mM NaCl, 1 mM EDTA pH 8, 1% Triton X-100 supplemented with cock-tail protease inhibitors (Roche Diagnostics). Protein concentration was finally determined by Bradford assay (Bio-Rad). Denaturation and reduction of protein samples of SDS-PAGE was performed at 37°C for 30 minutes. For each sample, 35 µg of total protein was loaded into 8% SDS gel and blotting was performed using a 0.45 µm nitrocellulose membrane (GE Healthcare). The blots were blocked for 1 hour with 5% non-fat dry milk prepared in TBST (10 mmol/L Tris (pH 8),

150 mmol/L NaCl, 0.1% Tween 20). They were subsequently incubated with primary antibodies for GFP (rabbit polyclonal, Abcam) and Tubulin (mouse monoclonal, Abcam) as a protein loading control, for 1 hour at room temperature. After that, they were washed three times in TBST and further incubated for 1 hour with secondary antibodies HRP-conjugated goat anti-rabbit (Santa Cruz) and anti-mouse IgG (Santa Cruz). Bound antibodies were detected by the ECL detection system (Santa Cruz). Densitometric analysis was performed using ImageJ 1.47v software.

### ***iPSC generation***

To generate iPSCs,  $1 \times 10^6$  fibroblasts were transfected with a total of 1  $\mu$ g of each episomal plasmids containing pCXLE-hOCT3/4-shp53-F, pCXLE-hSK, pCXLE-hUL (Addgene) (Okita K. *et al.*, 2011) — a more efficient method to generate integration-free human iPS cells. Electroporation was carried out using a Nucleofector™ 2b Device (Lonza) employing NHDF Nucleofector Kit (Lonza), following the manufacturer's instructions. After electroporation, the cells were cultured for 4 days in fibroblast medium and were then plated on mitomycin inactivated fibroblasts (feeder). The next day, the medium was switched to hES medium as follows: KO-DMEM, 20% Knock-out acids, 50 U/ml (penicillin and 50 mg/ml streptomycin), 100  $\mu$ M 2-mercaptoethanol (all from Invitrogen), and 10 ng ml<sup>-1</sup> bFGF (Peprotech). The medium was changed on alternative days until the formation of iPSC colonies (20-22 days). Then, individual iPSC colonies were manually picked and transferred to a new dish on mitomycin inactivated fibroblasts. The iPSCs were expanded by splitting them with collagenase (Invitrogen) and then frozen in liquid nitrogen in FBS (Hyclone) containing 10% DMSO (Sigma). To remove feeder from iPSC clones, the cells were grown for multiple passages (>5) on Matrigel (BD Biosciences) coated plates in mTeSR medium (Stem cell technologies).

### ***Generation of HLCs from iPSCs***

To generate hepatocytes from both control and patient iPSC clones, we employed an already described method that enables the efficient production of HLCs (Si-Tayeb K, *et al.*, 2010). Briefly, iPSC clones were plated on Matrigel and cultivated for 20-22 days. The media composition was changed as follows: 5 days in RPMI media supplemented with B27 and

100ng/ml of Activin A (R&D), 5 days in RPMI media supplemented with 20ng/ml BMP4 (R&D) and 10ng/ml bFGF (Preprotech), 5 days in RPMI-B27 supplemented with 20ng/ml hepatocyte growth factor (HGF, Invitrogen), and, finally, further 5-7 days in hepatocyte culture medium (Lonza) supplemented with 20ng/ml Oncostatin M (Invitrogen).

### ***Immunofluorescence of hiPSCs and HLCs***

hiPSCs were fixed in 4 % paraformaldehyde, permeabilized with 0.2 % TX-100 in 10 % FBS/1 % BSA in 1× PBS for 7 minutes at room temperature; non-specific signals were blocked in 10 % FBS/1 % BSA in 1× PBS for 30 minutes at room temperature. Thus, the cells were incubated with primary antibodies in 10 % FBS/1 % BSA in 1× PBS over night at 4°C. The following primary antibodies were used: anti-Oct4 (Santa Cruz), anti-Nanog (Cell Signaling), anti-alpha-fetoprotein (AFP) (Abcam), and anti-alpha-1 antitripsin (AAT) (Dako). After primary antibody incubation and washes in 1X PBS, the cells were incubated with the Alexa- Fluor 488 or 594 secondary antibodies (Molecular Probes) and the nuclei were stained with Dapi (Calbiochem). Cells were visualized with a 20×/0.40 (dry lens) objective using an inverted microscope (DMI4000, Leica Microsystems) at room temperature in 1× PBS. The images were captured with a digital camera (DFC365 FX, Leica Microsystems) using LAS-AF software (Leica Microsystems).

### ***Preparation of cell extracts, SDS-PAGE and Western blot analysis of HLCs***

After 20 days of differentiation, HLCs from control and patient iPSCs were treated with or without 100µM cycloheximide (Sigma) for the indicated time period. Cells were lysed with lysis buffer containing 10 mM Tris-HCl pH 7.4, 150 mM NaCl, 1 mM EDTA pH 8, and 1% Triton X-100 supplemented with cock-tail protease inhibitors (Roche Diagnostics); protein concentration was finally determined by Bradford assay (Bio-Rad). Denaturation and reduction of protein samples of SDS-PAGE was performed at 37°C for 30 minutes. For each sample, 35 ug of total protein was loaded into 8% SDS gel and blotting was performed using a 0.45 µm nitrocellulose membrane (GE Healthcare). The blots were blocked for 1 hour with 5% non-fat dry milk prepared in TBST (10 mmol/L Tris (pH 8), 150 mmol/L NaCl, 0.1% Tween 20). They were subsequently incubated

with primary antibody for ATP7B (rabbit polyclonal, Abcam) and Actin (rabbit polyclonal, SIGMA) as a protein loading control, for 1 hour at room temperature. Blots were washed thrice in TBST and further incubated for 1 hour with secondary antibodies HRP-conjugated goat anti-rabbit (Santa Cruz) and anti-mouse IgG (Santa Cruz). Bound antibodies were detected by the ECL detection system (Santa Cruz). Densitometric analysis was performed using ImageJ 1.47v software.

## 4. RESULTS

### 4.1 Generation of phosphomimic and phosphodeficient CryAB forms

We investigated the effects of phosphorylation on the chaperone activity of CryAB against misfolded TMPs. To this aim, we generated phosphomimic and phosphodeficient constructs of CryAB with an N-terminal FLAG tag by replacing the relevant serine residues with aspartic acid through site-directed mutagenesis. As shown in Fig. 14, the serine residues in position 19, 45, and 59 were all substituted with aspartic acid (CryAB-S3D) to mimic phosphorylation or with alanine residues (CryAB-S3A) to prevent it. Moreover, we further mutagenized the CryAB-S3A construct to generate either the single pseudo-phosphorylated CryAB-S19D, -S45D and -S59D mutants or the double pseudo-phosphorylated CryAB-S19/45D, -S19/59D and -S45/59D. Such procedure, allowed us to discern between the functional contribution of the single phosphomimetic residues and the coupled residues, having previously prevented phosphorylation at the other relevant serines. In addition, as a negative control for CryAB chaperone activity, we generated and used CryAB-R120G, a mutant defective in chaperone activity causing aberrant desmin folding and consequent related myopathy (Treweek T.M. *et al.*, 2005).

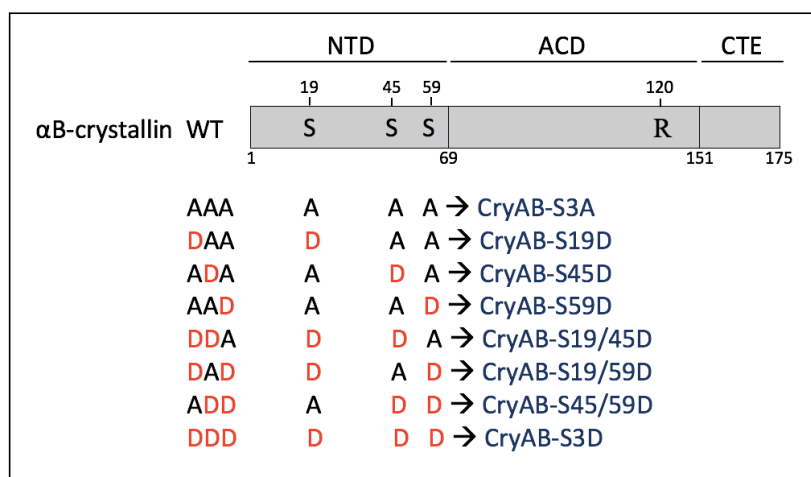


**Figure 14. Diagram of the mutant forms of CryAB generated and used this thesis.** The position of the relevant serine residues and arginine 120, and the boundaries between the domains are indicated. NTD, ACD, and CTE: N-terminal, Crystallin and C-terminal domains, respectively.

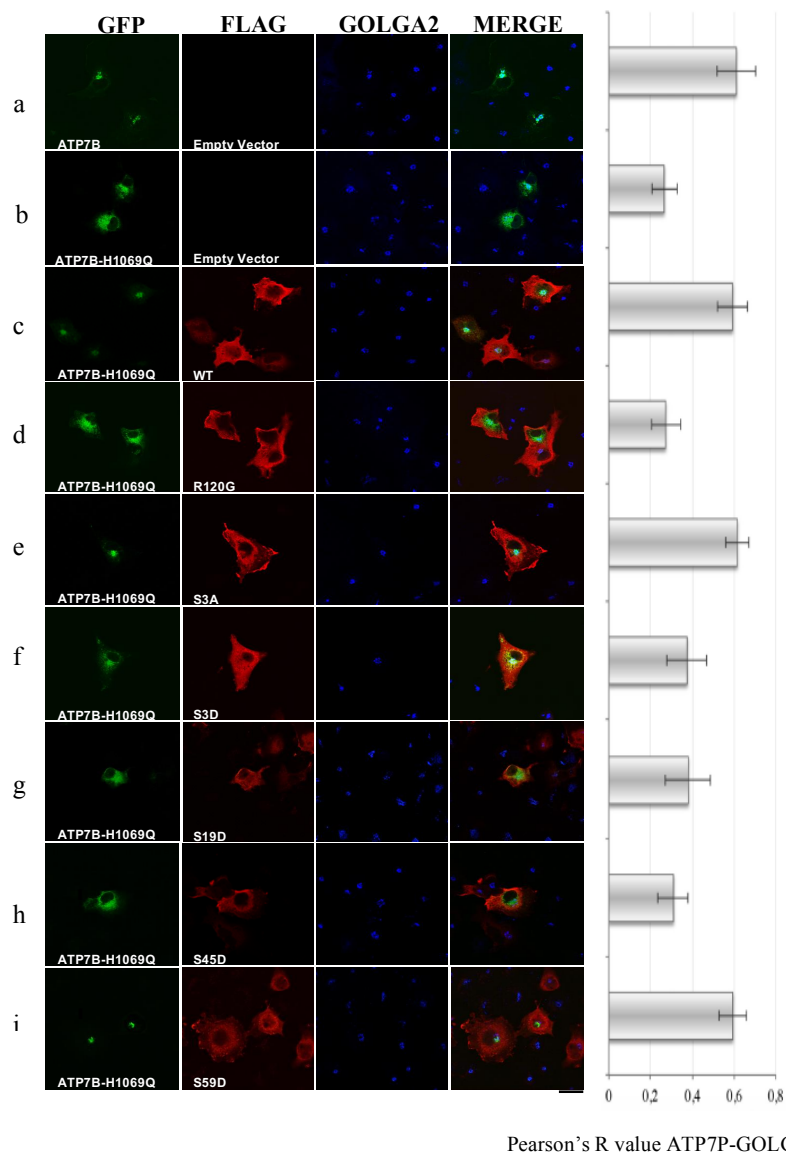
## 4.2 Mimicking phosphorylation of $\alpha$ B-CryAB affects its chaperone function

In a previous study, we demonstrated that ATP7B-H1069Q, assisted by CryAB but not CryAB-R120G, folds into the proper conformation, moves to the Golgi complex, and responds to Cu overload in the same manner as wild-type ATP7B in COS7 cells (D'Agostino M. *et al.*, 2013). This ATP7B-H1069Q mutant accumulates in the ER as misfolding aggregates (Dmitriev O.Y, *et al.*, 2011). Thus, to evaluate the effects of phosphorylation on CryAB chaperone activity, COS7 cells were either transiently transfected to express GFP-tagged ATP7B or ATP7B-H1069Q or co-transfected with wild-type CryAb, -R120G, or CryAB pseudo-phosphorylation mutants (Fig. 14). Confocal immunofluorescence microscopy showed that the ATP7B-H1069Q was mislocalized in comparison to ATP7B, which for the vast majority resides in the Golgi complex (Fig. 15 A, B). CryAB-S3A did not affect chaperone activity, thereby promoting ATP7B-H1069Q rescue to the Golgi as efficiently as the wild-type CryAb (Fig. 15 C, E). By contrast, CryAB-S3D exhibited only residual rescuing activity, thereby mimicking the inactive mutant -R120G (Fig. 15 D, F). At this point, we wondered which of the three serine residues, when phosphorylated, could equally and/or additively contribute to the negative regulation of the chaperone function. Interestingly, CryAB-S19D and -S45D showed only residual activity (Fig. 15 G, H), whereas the -S59D mutant was fully active (Fig. 15 I). Co-immunoprecipitation experiments showed that the phosphomimic constructs of CryAB-S19, -S45, -S59, and -S3D, as well as -R120G, bound to ATP7B-H1069Q, thus suggesting that the lack of activity was not due to loss of binding (D'Agostino M. *et al.*, 2013).

Next, to generalize these results, we performed the same experiment using the Frizzled4 (Fz4) receptor mutant (Fz4-FEVR), which is associated with a rare form of Familial exudative vitreoretinopathy (FEVR). In this mutant, a frameshift mutation (L501fsX533) generates a different and shorter C-terminal cytosolic tail of the receptor that accumulates in the ER of transfected cells (Robitaille J. *et al.*, 2002), preventing it from reaching the PM as does the wild-type FZ4. In this regard, we have previously shown that CryAB prevents the formation of inter-chain disulfide bridges of FZ4-FEVR aggregates in the ER, allowing for correct folding and appropriate localization on the PM of this mutant (D'Agostino M. *et al.*, 2013). In particular, in the presence of CryAB, FZ4-FEVR is almost fully rescued to the PM. By contrast whereas only a minor rescue was observed when CryAB-S3D, -S19D or -S45D replaced CryAB, both CryAB-S3A and -

S59D exhibited a strong rescue effect, only slightly below the wild type (Fig. 16). These findings strongly confirmed those obtained with ATP7B-H1069Q, suggesting that phosphorylation plays a pivotal role in CryAB chaperone activity toward TMPs.

Next, we asked whether different combinations of pseudo-phosphorylation could differently affect CryAB chaperone function. To this end, we generated double pseudo-phosphorylated mutants of CryAB (Fig. 17) assayed for chaperone activity by co-transfection with the ATP7B-H1069Q in COS7 cells. We demonstrated that the S19/45D resulted almost inactive whereas both S19/59D and S45/59D were close to the full active wild type CryAB. These results indicate not only that pseudo-phosphorylated S19 and S45 have an exclusive inhibitory role, but also that pseudo-phosphorylation at S59 has a protective effect toward the single pseudo-phosphorylation of S19 and S45, but not toward both simultaneously.



Pearson's R value ATP7P-GOLGA2)

**Figure 15. CryAB-S59D restores ATP7B-H1069Q localization in the Golgi complex, whereas CryAB-S19D, CryAB-S45D and the triple pseudo-phosphorylated CryAB-S3D do not.** COS-7 were co-transfected to express the indicated GFP-ATP7B forms (first column on the left) and the indicated 3xFLAG-tagged CryAB constructs or the control empty vector (second column from the left). 48 h post-transfection immunofluorescence analyses were performed. The anti-Golgin polyclonal GOLGA2 antibody was used to visualize the Golgi complex (third column from the left). Colocalization of GFP and GOLGA2 signals was determined with the ImageJ; the obtained Pearson's R value is shown on the right (mean  $\pm$  s.d., n. 10 cells of randomly selected fields from two independent experiments). Scale bar: 10  $\mu$ m (Ciano M. *et al.*, 2016).

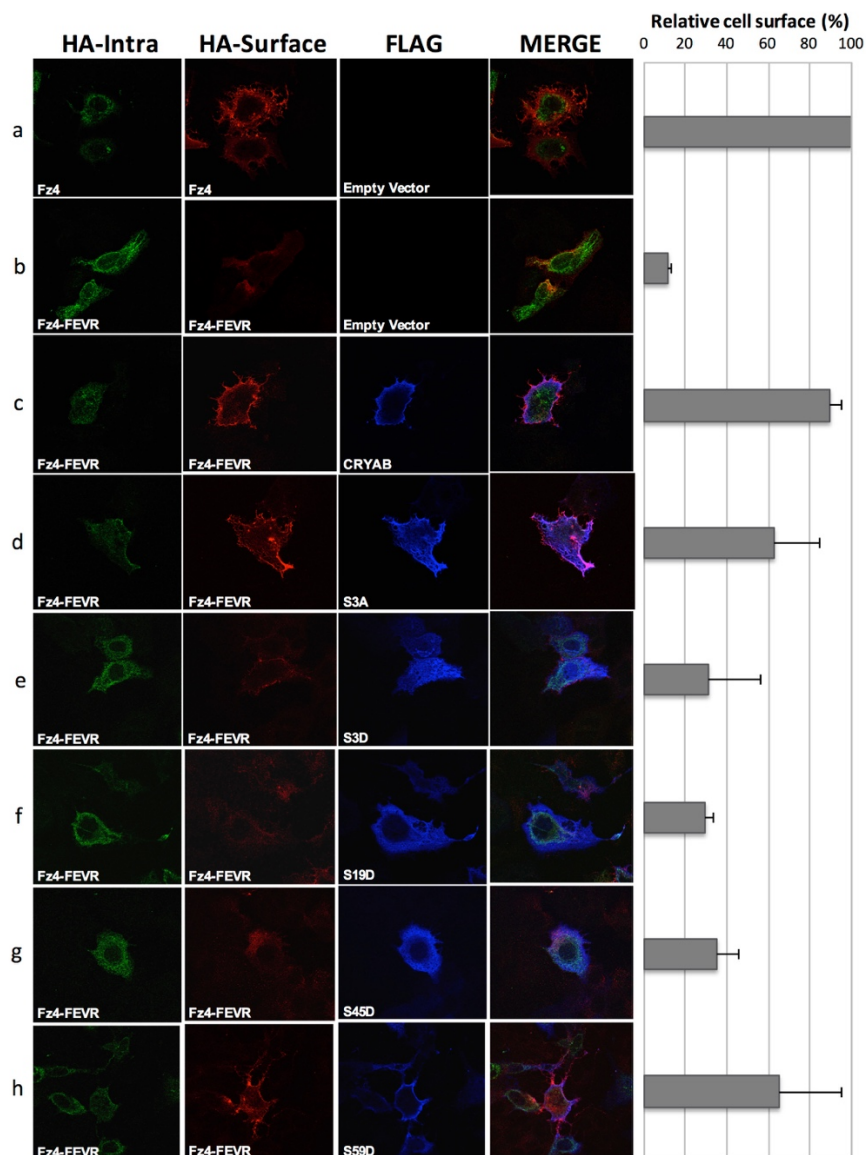


**Figure 16. CRYAB-S59D restores FZ4-FEVR localization in the plasma membrane, whereas CRYAB-S19D, CRYAB-S45D, and the triple pseudo-phosphorylated CRYAB-S3D do not.** Huh-7 cells were co-transfected to express the indicated HA-tagged FZ4 forms (first two columns on the left) and the indicated 3xFLAG-tagged CryAB constructs or the control empty vector (third column from the left). 48 h post-transfection the immunofluorescence analyses were performed to evaluate the presence of FZ4 forms on the PM. The histogram on the right shows for each row the surface ratio versus intracellular labeling (OUT/IN) of the FZ4 forms normalized to FZ4 wild type (mean  $\pm$  s.d., n = 10 cells from randomly selected fields of two independent experiments). Scale bar: 10  $\mu$ m (Ciano M. *et al.*, 2016).

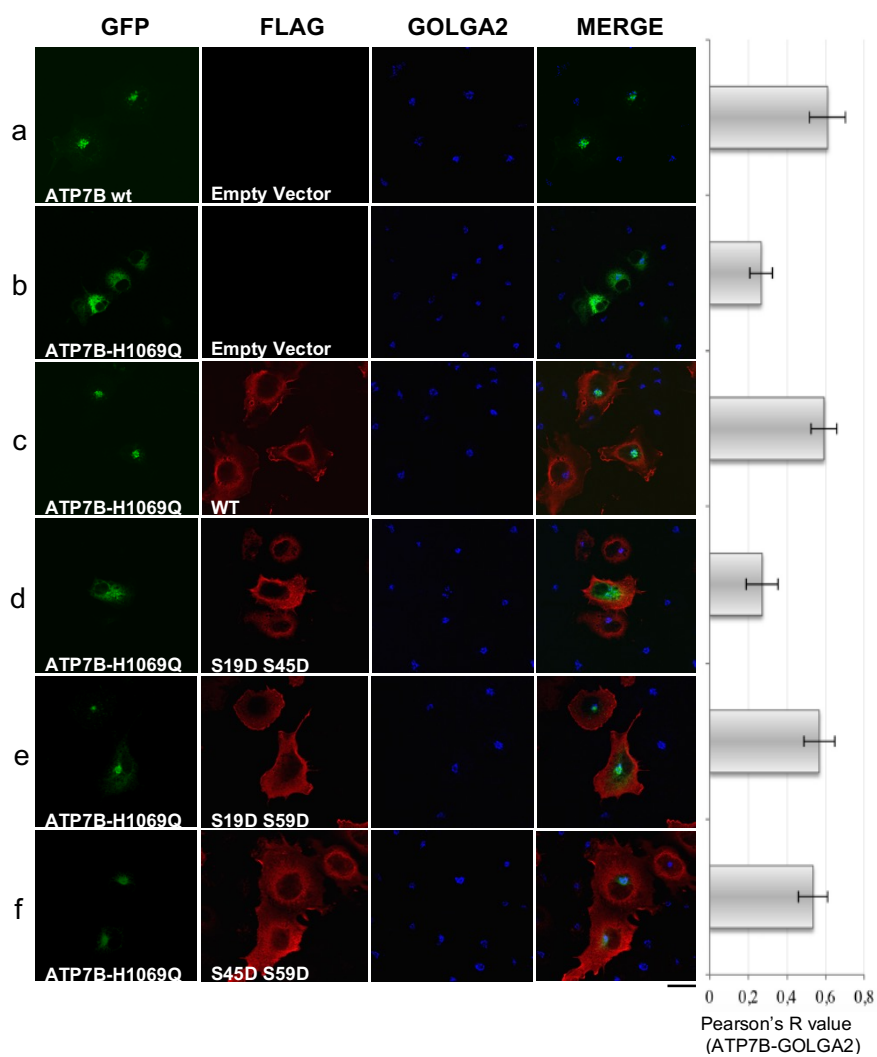


**Figure 17. The pseudophosphorylated S59D protects CryAB chaperone activity in double pseudophosphorylated mutants.** Cells were manipulated and analyzed as in Fig. 15 (Ciano M. *et al.*, 2016).

### 4.3 Pseudo-phosphorylation reduces the oligomerization state of CryAB

Previous studies have reported that CryAB chaperone activity, similarly to Hsp27, is correlated with the size of its oligomeric complexes (Aquilina J.A. *et al.*, 2004; Ito H. *et al.*, 2001; Arrigo A.P. *et al.*, 2007). Because phosphorylation of serine residues negatively interferes with the degree of oligomerization and chaperone activity (Bakthisaran R. *et al.*, 2016), we asked whether the different contribution of phosphorylated serines to CryAB chaperone activity could derive from a diverse impact on the oligomerization state of the chaperone. To answer this question, we transiently transfected cells with different phosphomimetic mutants and analyzed them by sedimentation assay in glycerol gradient, SDS-PAGE, and immunoblotting. The results showed that (Fig. 18), almost 2/3 of total CryAB sediments in the heavier region of the gradient, as well as CryAB-R120G. Most important, whereas CryAB-S3D is slightly enriched in the lighter region, CryAB-S3A is equally present in the two regions. Interestingly, all three single phosphomimetic mutants -S19D, -S45D, and -S59D are clearly enriched in the lighter fractions. The two pseudo-phosphorylated CryAB-S19D and -S45D single mutants show only residual activity (Fig. 15G, H), while the -S59D mutant results fully active (Fig. 15 I). Thus, the inhibitory effect seen for S19 and S45 cannot be ascribed to the reduction of oligomerization. Altogether, these data demonstrate that the reduction of the oligomerization state of CryAB does not correlate with the inhibition of its chaperone activity, suggesting a direct role, yet to be elucidated, of phosphorylation in controlling CryAB chaperone activity.

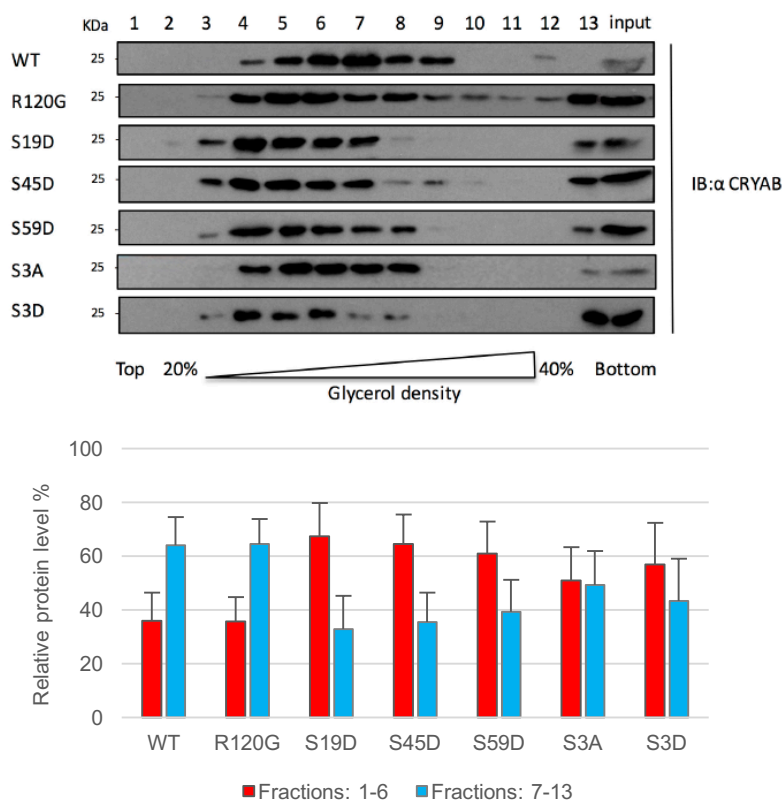


**Figure 18. All pseudophosphorylated CryAB forms determine the formation of smaller oligomeric complexes.** COS7 cells were transfected to express the indicated 3xFLAG-tagged CryAB forms. Forty-eight hours post-transfection, the cells were lysed and aliquots of the cell extracts were analyzed on of 20-40% glycerol gradients. The gradients were collected in 12 fractions (fraction 13 is the resuspended pellet) and the protein content resolved on 12% SDS-PAGE followed by immunoblotting to detect CryAB (25kDa). One representative immunoblotting result is shown. Quantitative analysis of the distribution of CryAB forms in fractions 1-6 and 7-13 of the glycerol gradients (mean  $\pm$  s.d., n. = 3-6 independent experiments) is shown in the histogram below (Ciano M. *et al.*, 2016).

#### 4.4 $\alpha$ -Crystallin domain rescues Golgi localization of ATP7B-H1069Q mutant

Since D'Agostino *et al.* demonstrated that CryAB is able to interact with ATP7B-H1069Q and rescue its proper intracellular localization (D'Agostino M. *et al.*, 2013), we set out to identify which specific region of CryAB maintains this functional role (chaperone activity). A previous report showed that the isolated domains maintain some level of chaperone activity in vitro (Asomugha CO. *et al.*, 2011). Accordingly, we dissected CryAB in its main domains. N-terminal (NTE),  $\alpha$ -crystallin (ACD), and C-terminal (CTE) domains (residues 1-66, 65-146, 148-175, respectively) were cloned in a HAN(I)pcDNA3 vector to generate HA-tagged constructs. Then, to determine which CryAB domains were able to rescue Golgi localization of ATP7B mutant, we transiently transfected COS7 to express GFP-tagged ATP7B or ATP7B-H1069Q or co-transfected them with wild-type CryAb or HA-tagged CryAB. Confocal immunofluorescence analysis revealed that when ATP7B-H1069Q is co-transfected with the N-terminal (NTE) or C-terminal (CTE) domain, no rescue effect is obtained as the mutated protein is retained in the ER. In contrast, the  $\alpha$ -crystallin domain (ACD) markedly recovers the intracellular compartmentalization of ATP7B-H1069Q, as evidenced by its high expression in the Golgi (Fig. 19). These results strongly suggest that only the  $\alpha$ -crystallin domain (ACD) is able to rescue ATP7B-H1069Q Golgi-localization as efficiently as the full-length CryAB. To further confirm these data, we evaluated the colocalization of GFP and GOLGA2 signals with the ImageJ colocalization plugin; the obtained Pearson's R value is shown in the histogram below.

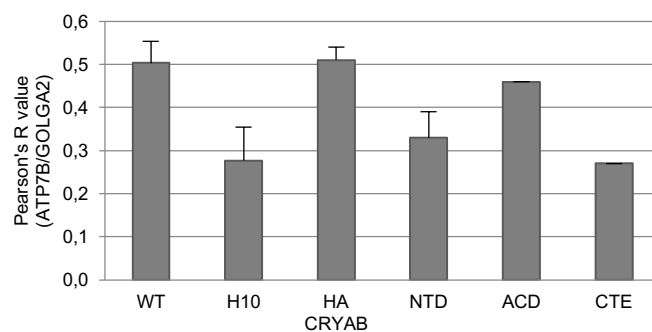
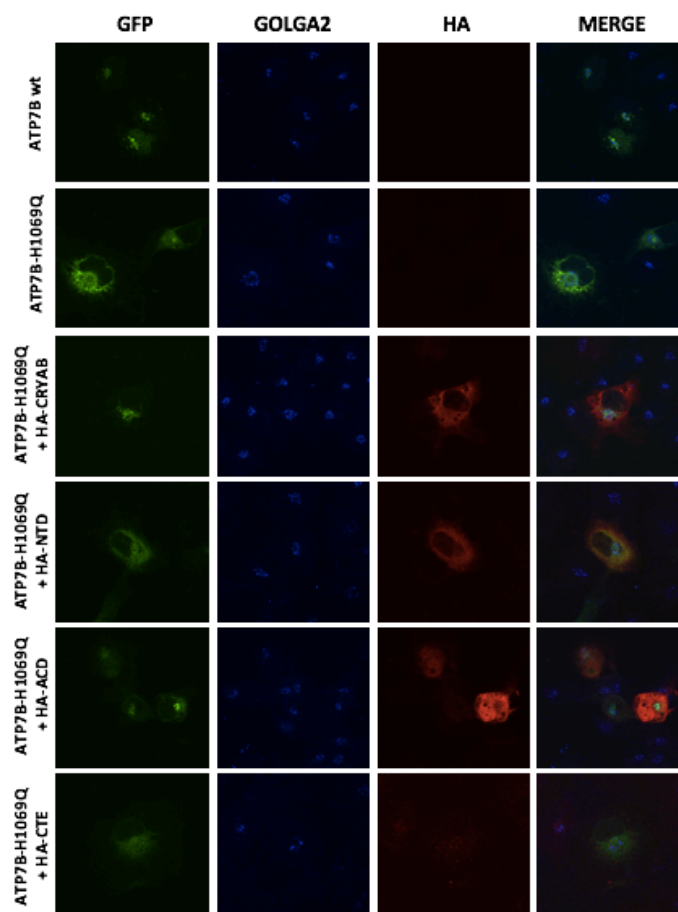


**Figure 19.  $\alpha$ -Crystallin domain corrects localization of ATP7B-H1069Q from the ER to the TGN.** COS7 cells were transfected to express GFP-tagged ATP7B or ATP7B-H1069Q or co-transfected with HA-CryAB or its domains (HA-NTE, HA-ACD and HA-CTE respectively). The histogram shows the colocalization of GFP and GOLGA2 signals determined with Pearson's R using the ImageJ software (mean  $\pm$  s.d., n. 10 cells of randomly selected fields from two independent experiments). Scale bar: 10  $\mu$ m.

#### 4.5 CryAB peptide does not affect cell viability

In light of previous results, it is clear that CryAB crystallin-domain, as well as the full-length protein, is able to counteract aggregation and to rescue the proper intracellular localization of the mutated Cu transporter ATP7B-H1069Q (D'Agostino M. *et al.*, 2013). Furthermore, several papers have also demonstrated that CryAB peptides derived from the crystallin domain exert a holdase activity *in vitro*. Most important, CryAB peptide corresponding to residues 73-92 protects human lens epithelial (HLE) cells from thermal stress-induced apoptosis and inhibits selenite-induced cataracts after intraperitoneal injection in rats (Nahomi *et al.*, 2013). Based on this evidence, we used the syntetic peptide 73-92 (Peptide1) and control peptides (Peptide2, inverted sequence; Peptide3, scrambled) to verify whether this CryAB-derived peptide was able to mimic the effect of the crystallin domain and the full-length protein on ATP7B-H1069Q. To this aim, we either labeled or unlabeled these peptides with TAMRA at the side chain amino group of Lysine residue at the carboxy (Pept1) and amino terminal ends (Ctrl Pept), respectively (Fig. 20). In brief, to assess whether the peptide 73-92 and the control peptide were toxic to our cellular systems, we performed an MTT assay on two different cell lines: COS7 and HepG2 KO. These cells were incubated with 12.5  $\mu\text{M}$  of Pept1 and Ctrl Pept for 96 and 120 hours. We observed that in both COS7 and HepG2 cells, Pept1 and Ctrl Pept did not affect cell viability at the indicated times of incubation compared to untreated cells (Fig. 21). Then, to further confirm these data, we set up a cell growth curve by treating HepG2 cells with either Pept1 or Ctrl Pept. Cells were counted after 24, 48 and 72 hours. After 72 hours, peptides were readministered and cells were recounted two days later. After each count, we found that both peptides did not impair cell division and proliferation, thereby strongly indicating that peptide treatment is safe for the cellular systems used and, more broadly, for our particular cellular system (Fig. 21).

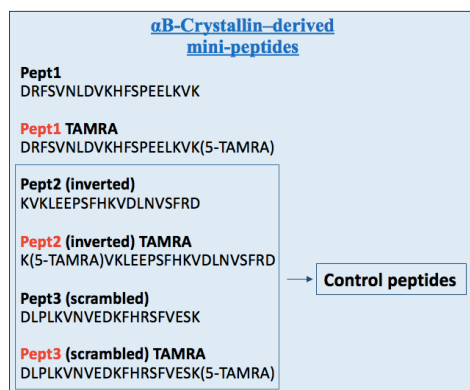


**Figure 20.  $\alpha$ B-Crystallin-derived mini-peptides.** Schematic representation of  $\alpha$ B-crystallin-derived peptide sequence (Pept1) and the control peptides (Peptide2, inverted sequence; Peptide3, scrambled) labeled or unlabeled with TAMRA.

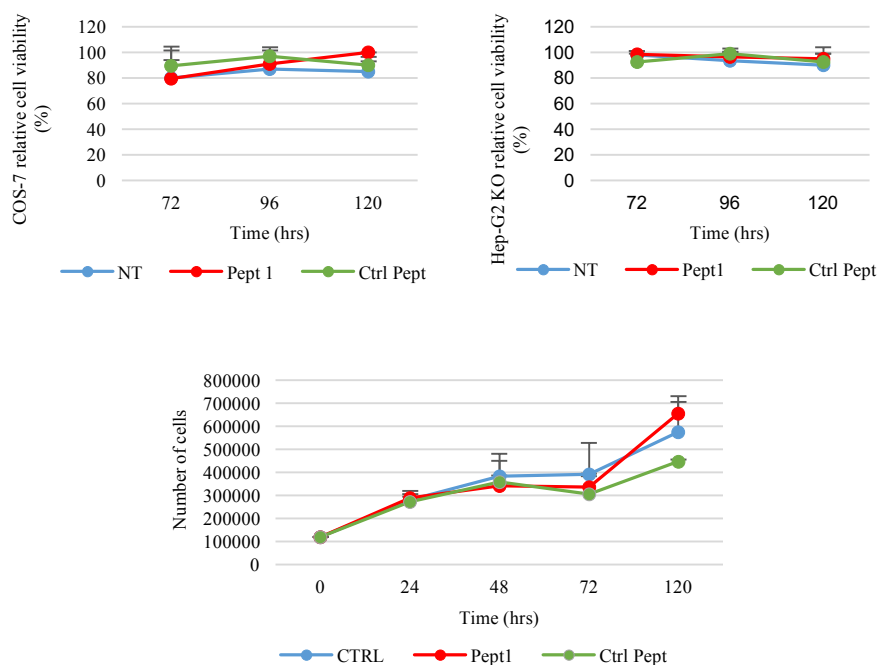


**Figure 21. CryAB peptide does not affect cell viability.** Cell survival of COS7 and HepG2 KO cells was determined by MTT assay after 72, 96, and 120 hours of peptide exposure (graphs above) and by cell count after 24, 48, 72, 120 hours of peptides exposure in HepG2 KO cells (graph below). MTT assay revealed that peptides treatment did not reduce cell viability. No significant differences were observed in the increase of cellular number after prolonged peptide exposure in comparison with the control. MTT and growth curve data are represented as mean  $\pm$  s.d of at least 3 independent experiments.

#### 4.6 Internalization of CryAB peptide

Since CryAB and control peptides do not impair cell viability, we asked whether these peptides could be internalized by the cells. To answer this question, we incubated COS7 cells with 12.5  $\mu\text{M}$  of TAMRA labeled Pept1 and Ctrl Pept for 1, 4, and 20 hours. Using confocal immunofluorescence microscopy, we observed that the peptide fluorescent signal became cytosolic after about 4 hours and partially colocalized with the lysosomal marker LAMP-1 after 20 hours (Fig. 22) (Allocca Simona's Ph.D thesis. New Therapeutic Perspectives for the Most Frequent ATP7B Mutation in Wilson Disease: Development of Pharmacologically Active Peptides and Generation of a Novel WD Isogenic Cell Model).

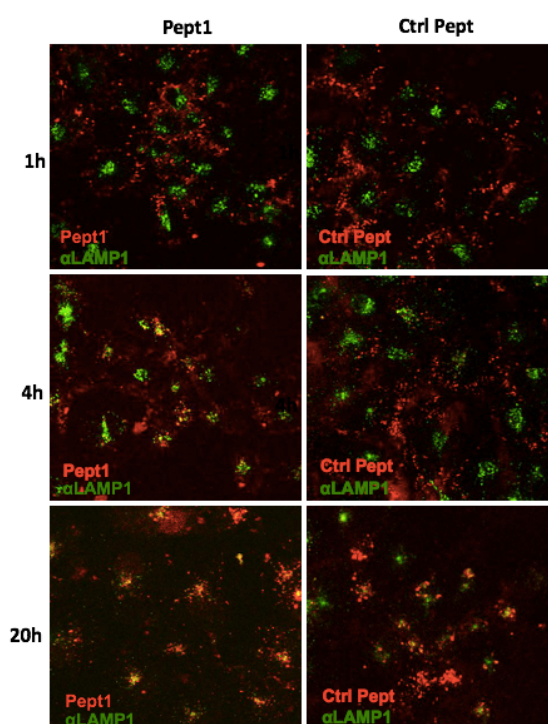


**Figure 22. Peptide fluorescent signal colocalizes with the lysosomal marker.** COS7 cells were incubated with 12.5  $\mu\text{M}$  of TAMRA-labeled Pept1 and Ctrl Pept at the indicated times. Confocal immunofluorescence analysis were performed with an anti-LAMP1 protein antibody to visualize the lysosomes. Peptide fluorescent signal was evident in the cytosol after about 4 hours and co-localization with LAMP1 was predominant after 20h. Scale bar: 10  $\mu\text{m}$ .



#### 4.8 *Pept1*, but not *Ctrl Pept*, rescues the Golgi localization of *ATP7B-H1069Q*

To assess whether CryAB-derived peptides were able to rescue the proper localization of ATP7B-H1069Q, as already seen with the crystallin domain and the full-length protein, COS7 cells were either transfected to express GFP-tagged ATP7B and ATP7B-H1069Q, or co-transfected with wild-type CryAB as control. Next, these cells were treated with Pept1 and Ctrl Pept conjugated or unconjugated to TAMRA for 24 hours post transfection. We found that GFP-ATP7B wild type was expressed mainly in the Golgi complex, as indicated by co-localization with GOLGA2 marker (blu staining), whereas GFP-ATP7B-H1069Q was mainly expressed in the ER (Fig. 24). Therefore, we concluded that in cells expressing ATP7B-H1069Q and co-transfected with the full-length CryAB or treated with Pept1 (labeled or unlabeled with TAMRA), ATP7B-H1069Q rescues the TGN localization (Fig. 24). No such effects were observed in cells co-transfected with CryAB-R120G (data not shown) or treated with Ctrl Pept (Fig.24). To further corroborate these data, we used confocal immunofluorescence microscopy to evaluate the colocalization of GFP and GOLGA2 signals with the ImageJ colocalization plugin; the obtained Pearson's R value is shown in the graph below (Fig. 24). These results show that Pept1 exerts a similar effect to full-length CryAB.

It is in the wake of this important new evidence that we decided to look for a cellular model that would more closely mimic WD. First, we considered using human hepatocytes. However, despite remaining the gold standard for WD molecular analysis in the liver, their availability is very limited. Second, we took into consideration human hepatoma cell lines, which are indeed excellent cellular platforms to study ATP7B and its role in Cu homeostasis, as exemplified by the most widely studied hepatic cell line, Huh7 (Huster D. *et al.*, 2003; Song MO. and Freedman JH. 2005). However, a major drawback of using this cell line is that the Huh7 and the other human hepatic cell lines, like HepG2 and Hep3B, express the endogenous, functional ATP7B, a property that can interfere with the localization of ATP7B-H1069Q (Lutsenko S. *et al.*, 2007).

Thus, in the end, we did the same experiment using the HepG2 KO hepatic cell line, which does not express ATP7B (data not shown) (Allocca Simona Ph.D thesis) and Huh7 (Fig. 25). Not surprisingly, we obtained the same results as those obtained in COS7 cells, thereby confirming that Pept1 rescues the Golgi localization of ATP7B-H1069Q.

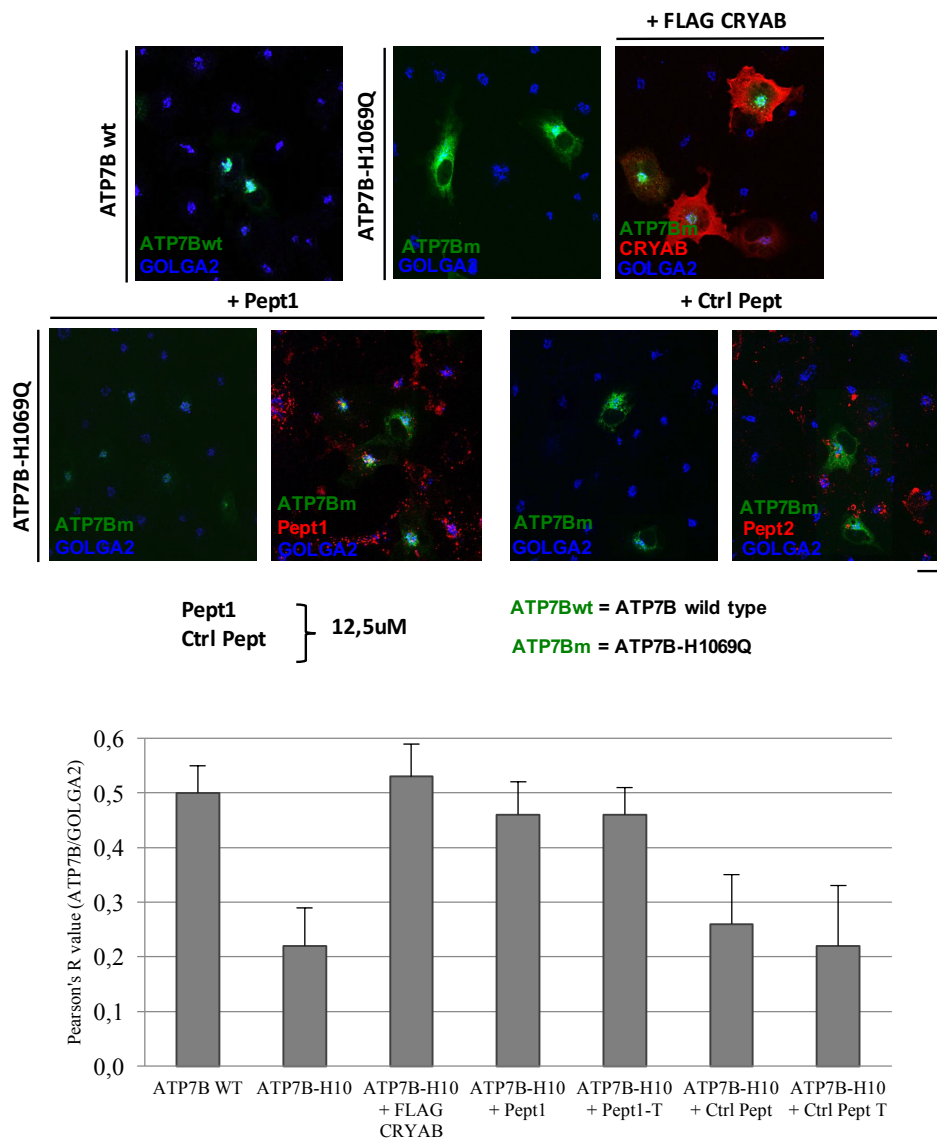


**Figure 24. Peptide1 corrects localization of ATP7B-H1069Q from the ER to the TGN in COS7 cells.** COS7 cells were transfected to express GFP-tagged ATP7B or ATP7B-H1069Q and co-transfected with 3xFlag-CryAB or incubated with Pept1 and Ctrl Pept (12.5  $\mu$ M) in the presence or absence of TAMRA for 24h post-transfection. Subsequently, confocal immunofluorescence analysis were performed using an anti-GOLGA2 protein antibody to visualize the Golgi complex. The histogram shows the extent of colocalization of both ATP7B and ATP7B-H1069Q with GOLGA2 (mean  $\pm$  s.d., n=20 cells from 3 independent experiments). Scale bar: 10  $\mu$ m.

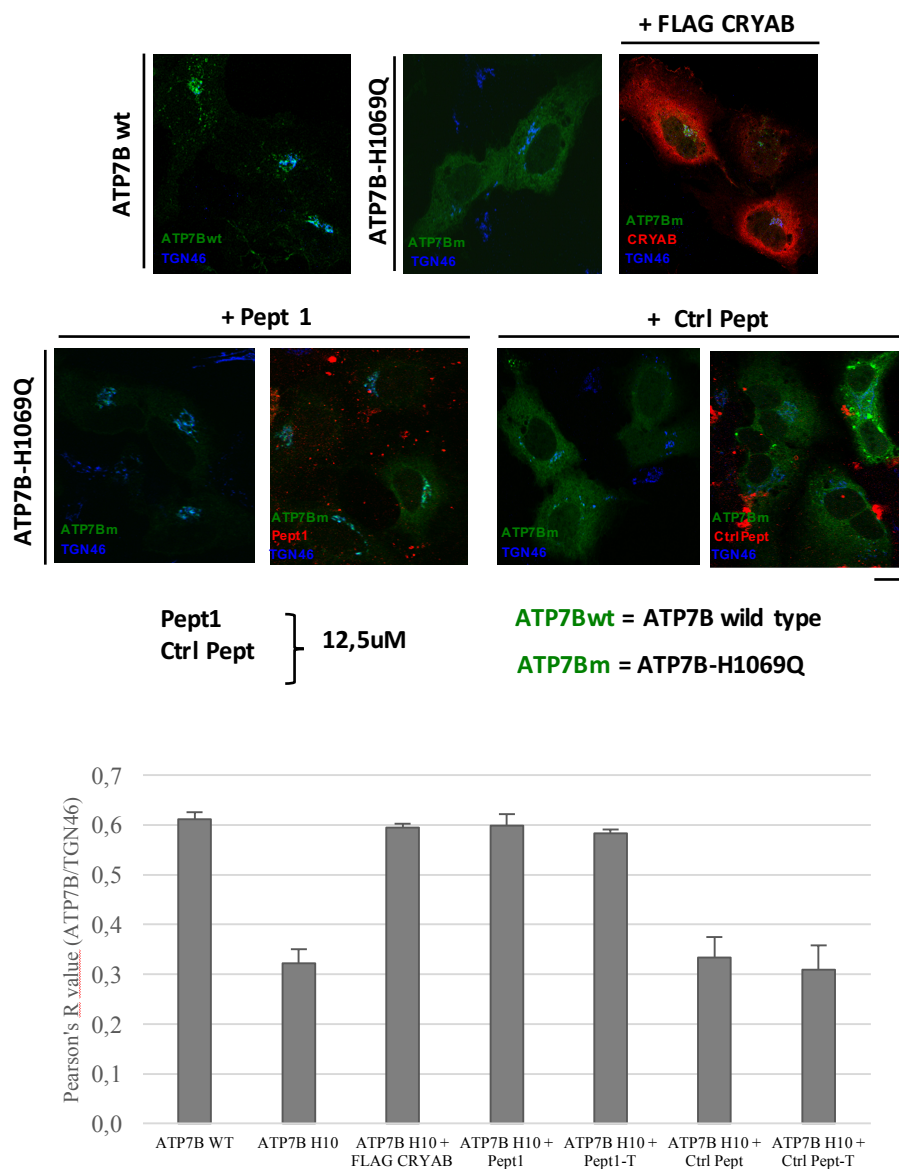


**Figure 25. Peptide 1 rescues Golgi localization of ATP7B-H1069Q in Huh7 cells.** Huh-7 cells were co-transfected to express GFP-tagged ATP7B or ATP7B-H1069Q and co-transfected with 3xFlag-CRYAB or incubated with Pept 1 and Ctrl Pept (12.5  $\mu$ M) in the presence or absence of TAMRA for 24 hours post-transfection. Subsequently, confocal immunofluorescence analyses were performed using an anti-TGN46 protein antibody to visualize the Golgi complex. The histogram shows the extent of colocalization of ATP7B and ATP7B-H1069Q with TGN46 (mean  $\pm$  s.d., n=30 cells from 3 independent experiments). Scale bar: 10  $\mu$ m.

#### ***4.9 The Golgi-corrected ATP7B-H1069Q moves to post-Golgi vesicles in response to Cu overload in the presence of Pept1***

In previous studies, we demonstrated that Pept1 retains the ability to rescue the Golgi localization of ATP7B-H1069Q, as efficiently as the isolated crystallin domain and full-length CryAB. Encouraged by these findings, we decided to investigate whether Pept1 Golgi-corrected ATP7B-H1069Q is also able to respond to copper overload.

To address this question, we transfected COS7 cells to express GFP-tagged ATP7B WT or ATP7B-H1069Q. Then, after 24 hours, we incubated them with 12.5  $\mu\text{M}$  of TAMRA-labeled or unlabeled Pept1 and Ctrl Pept. Next, we incubated them again for 2 hours in a medium containing either 200  $\mu\text{M}$  of  $\text{CuSO}_4$  or 500  $\mu\text{M}$  of bathocuproine disulphonate (BCS), a Cu chelator. Interestingly, our confocal immunofluorescence analysis using an anti-GOLGA2 antibody (Fig. 26) revealed that Pept1, just like the full-length CryAB, induces the Golgi-corrected ATP7B-H1069Q to move from post-Golgi vesicles in response to a Cu overload, similarly to ATP7B WT.

That Pept1 facilitates ATP7B-H1069Q response to Cu overload as efficiently as full-length CryAB, is illustrated below in Figure 26. In particular, the white spots indicate a Golgi localization of ATP7B and ATP7B-H1069Q in the presence of Pept1 using low Cu conditions, whereas a dispersed punctate staining pattern of ATP7B and ATP7B-H1069Q with Pept1 towards the cytosolic vesicular compartment is observed upon Cu exposure. In contrast, the Ctrl Pept does not show the same effect in the presence of excess Cu. The histogram (Fig. 26) shows an increase in ATP7B-H1069Q Golgi-localization in the presence of Pept1 without Cu and an increase in post-Golgi vesicles after Cu treatment.

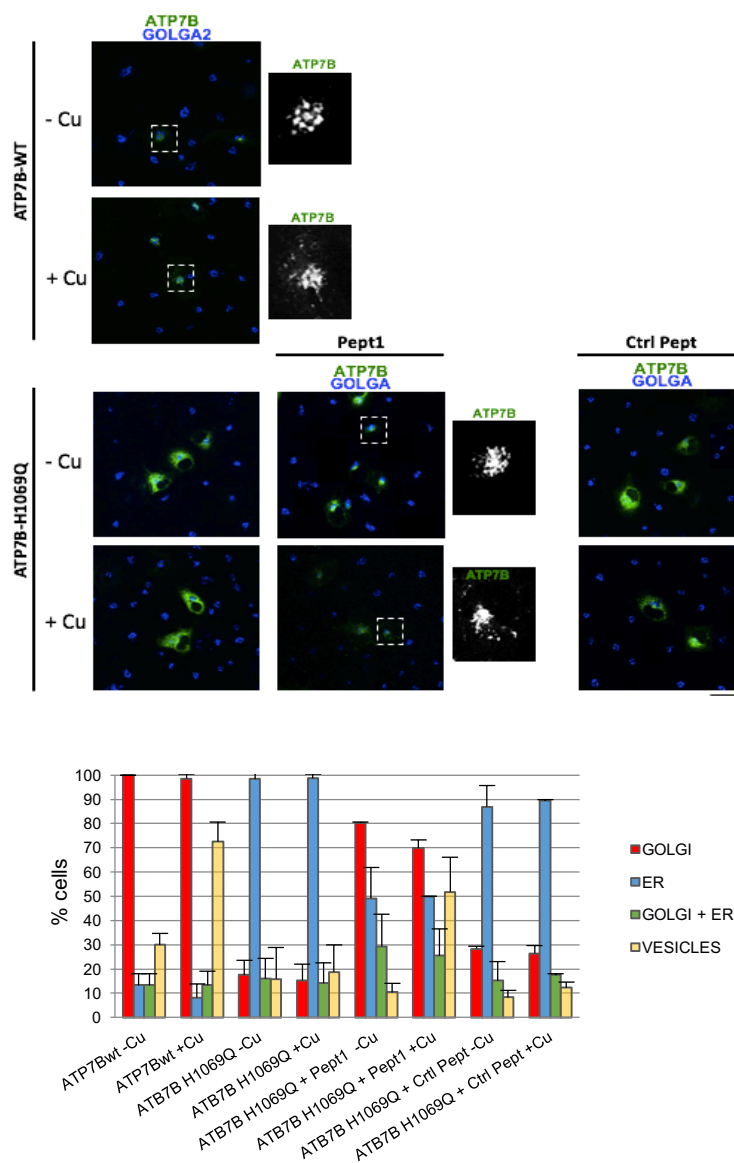


**Figure 26. ATP7B-H1069Q responds to Cu overload in the presence of Pept1.** COS7 cells were transfected to express GFP-tagged ATP7B or ATP7B-H1069Q and incubated with Pept1 and Ctrl Pept (12.5  $\mu$ M) for 24 hours post-transfection. Then, 2h before fixation, the cells were incubated with 200  $\mu$ M of  $\text{CuSO}_4$  (+Cu) or 500  $\mu$ M of bathocuproine disulphonate BCS (-Cu). Subsequently, confocal immunofluorescence analysis were performed using an anti-GOLGA-2 protein antibody to visualize the Golgi complex. The histogram shows the percentage of ATP7B or ATP7B-H1069Q transfected cells exhibiting ER, Golgi complex, ER + Golgi complex and PM + vesicular staining, respectively (average  $\pm$  s.d., n=25 cells from 2 independent experiments). Scale bar: 10  $\mu$ m.

#### ***4.10 Pept 1, but not Ctrl Pept, interacts with ATP7B WT and H1069Q***

To evaluate whether Pept1 would interact with ATP7B WT and H1069Q, we performed a co-immunoprecipitation assay. Co-immunoprecipitation is a technique commonly used to identify protein-protein interactions. Using a specific antibody as a target protein, we were able to indirectly capture the proteins that were bound to our protein of interest. Then, we analyzed the co-immunoprecipitation samples using nanoLC-ESI-Q-Orbitrap MS/MS.

COS7 cells were transfected to express GFP-tagged ATP7B WT or ATP7B-H1069Q and incubated with Pept1 and Ctrl Pept (12.5  $\mu$ M) labeled with TAMRA for 24 hours post-transfection. The obtained cell lysates were incubated first with primary antibody anti-GFP and then with Protein A-Sepharose beads. This protein was used because it is able to bind to the Fc region of the primary antibody. Proteins that are targeted by the antibodies are then captured onto the beads via Protein A and are easily recovered by low speed centrifugation. The immunoprecipitated samples were analyzed using nanoLC-ESI-Q-Orbitrap MS/MS by Chiara D'Ambrosio, a colleague working in the laboratory of Professor Scaloni at ISPAAM.

Pept1 and Ctrl Pept labeled with TAMRA had the same molecular mass (2798.41 Da as monoisotopic value) and the same mass spectra. However, because they had different amino acid sequences, we were able to distinguish them from their different fragmentation spectra. Since both their mass spectra showed prominent peaks at  $m/z$  560.69, corresponding to the quintuple charged ions, we monitored this value in the samples using the SIM mode to increase sensitivity.

Therefore, the presence or absence of the Pept1 in immunoprecipitated samples from ATP7B WT and H1069Q was checked by SIM-MS experiment. The selected ion monitoring chromatogram clearly showed the occurrence of a peak at 35 min corresponding to Pept1 (Fig. 27, Panels A and D), as ascertained by its MS/MS spectrum (Fig. 28), only in the ATP7B sample containing Pept1, and WT and H1069Q. No peaks related to the signal at  $m/z$  560.69 were revealed in the ATP7B samples containing control, WT and H1069Q, ATP7B without peptides, and WT and H1069Q (Fig. 27 Panels B, C, E, F).

These results were strongly supported by FLIM analysis (data not shown) (Allocca Simona's Ph.D thesis).

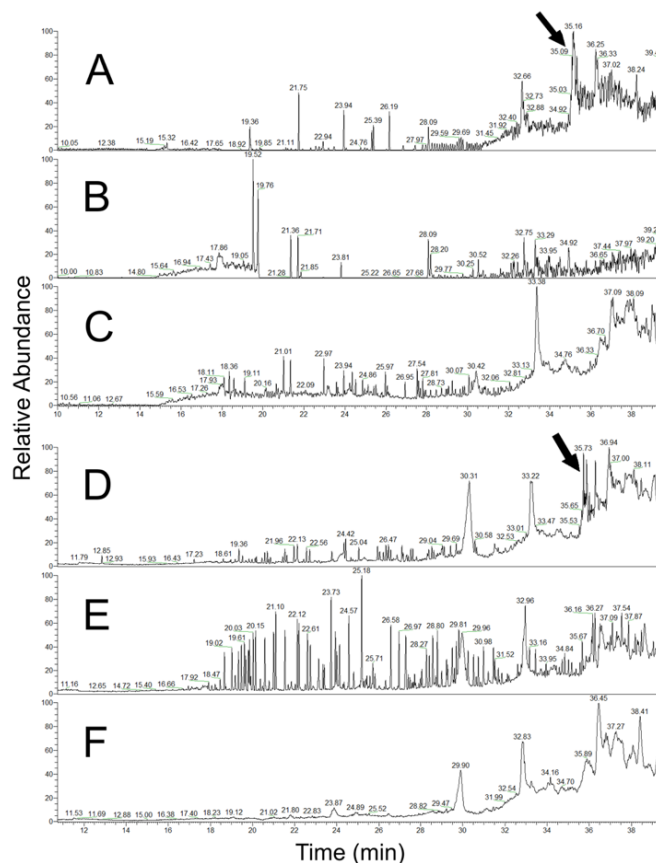


**Figure 27. NanoLC-ESI-Q-Orbitrap SIM-MS analysis.** Selected ion monitoring chromatogram ( $m/z$  560.69  $\pm$  0.6) of ATP7B WT + Pept1 (A) ATP7B WT + Ctrl Pept (B) ATP7B WT (C) ATP7B-H1069Q + Pept1 (D) ATP7B + Ctrl Pept (E) ATP7B-H1069Q (F). Peak really corresponding to Pept1 are marked with narrow arrows.

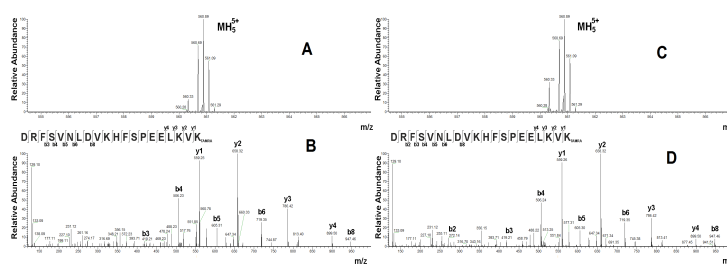


**Figure 28. Mass spectrum of the Pept1.** Mass spectrum of Pept1 (precursor quintuple charged ions at  $m/z$  560.69) from ATP7B WT + Pept1 (A) and its relative MS/MS spectrum (B). Mass spectrum of Pept1 from ATP7B-H1069Q + Pept1 (C) and its relative MS/MS spectrum (D).

#### 4.11 Pept1 increases ATP7B-H1069Q half-life

Since the H1069Q mutant has a decreased half-life compared with the wild-type ATP7B (Dmitriev OY. *et al.*, 2011), we asked whether Pept1 was also able to increase ATP7B-H1069Q half-life. To this end, HepG2 cell line knockout for the expression of ATP7B (HepG2 KO) were infected with GFP-ATP7B-H1069Q and incubated with 12.5  $\mu$ M of Pept1 and Ctrl Pept for 24 hours. We then treated the cells with protein synthesis inhibitor cycloheximide (Chx) (100  $\mu$ M) for 2 hours and performed Western blotting. We found that when HepG2 KO cells were infected with GFP-ATP7B-H1069Q, ATP7B-H1069Q expression level decreased after 2 hours of Chx treatment, as well as in the presence of Ctrl Pept, whereas HepG2 KO cells infected with GFP-ATP7B-H1069Q and treated with Pept1 did not. These data demonstrate that Pept1 is able to stabilize ATP7B-H1069Q, thereby increasing its half-life (Fig. 29).

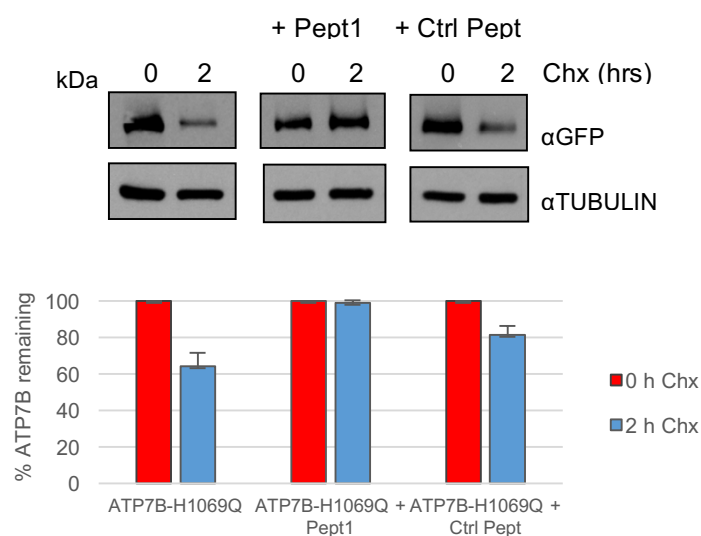


**Figure 29. Pept1 increases ATP7B-H1069Q half-life.** HepG2 KO cells were infected with GFP-ATP7B-H1069Q, incubated with 12.5  $\mu$ M of Pept1 and Ctrl Pept for 24 hours. Cells were then treated with Chx (100  $\mu$ M) for 2 h and Western blotting was performed. Tubulin was used as loading control. The level of remaining ATP7B was quantified as the percentage of initial ATP7B level (0 hour of Chx treatment), as shown in the histogram. Data are reported as means  $\pm$  SEM of two biological replicates.

#### 4.12 Generation of hepatic differentiation of WD and control hiPSCs

To generate hiPSCs, in collaboration with Dr. Silvia Parisi, Anna Musto, Simona Allocca and Prof. Roman Polishchuk, we obtained primary fibroblasts from skin biopsies of a homozygous H1069Q WD patient (H1069Q/H1069Q) and a familiar control (WT/H1069Q). iPSCs were produced using an integration-free method by transfecting episomal plasmid vectors into primary fibroblasts (Okita K. *et al.*, 2011), instead of retro or lentivirus, thus avoiding genetic integration and the risk of changing the genetic asset of the patient's cells. iPSC-like colonies emerged three weeks after transfection. Positivity for the stemness markers Nanog and Oct4 was assessed by immunofluorescence (Fig. 30).

In WD, the liver is the most affected organ in the body, being the site in which Cu homeostasis occurs and in which ATP7B is primarily expressed. Thus, we differentiated patient and control iPSCs into HLCs using a previously established protocol (Si-Tayeb K. *et al.*, 2010). This protocol mimics liver development by passing through three hepatic developmental stages: definitive endoderm, hepatic progenitors, and hepatocyte-like cells. We further differentiated them toward the hepatic lineage for 20 days, specifically until they resulted positive for hepatic cell markers such as albumin (ALB) (data not shown),  $\alpha$ -fetoprotein (AFP), and  $\alpha$ -1-antitrypsin (AAT) (Fig. 30).

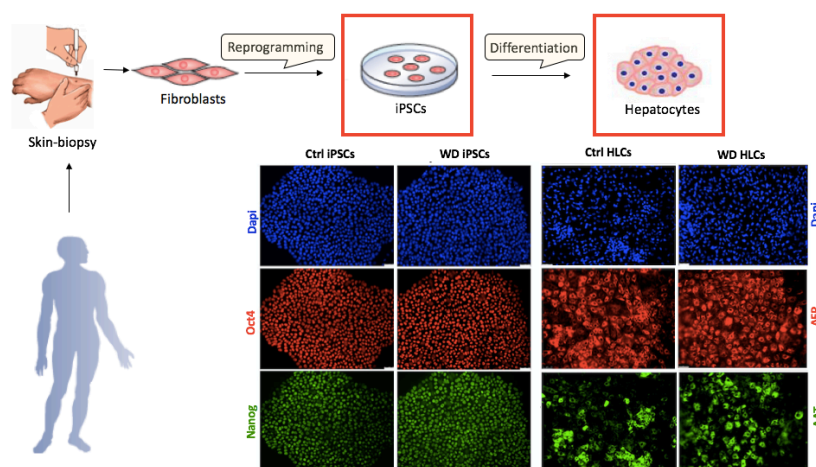


**Figure 30. Generation of hepatic differentiation of WD and control hiPSCs.** Control and WD patient-derived fibroblasts were reprogrammed to generate hiPSCs and then differentiated into HLCs. Immunofluorescence microscopy for stemness markers (Oct4 and Nanog) and hepatic cells markers (AFP and AAT) in a representative control and WD clone. Nuclei are stained in blue with DAPI. Scale bars: 50  $\mu$ m

#### 4.13 ATP7B expression in HLCs from patient and control hiPSCs

Overexpression studies have revealed that the mutant ATP7B-H1069Q is subjected to rapid degradation (Payne AS. *et al.*, 1998; van den Berghe P. V. *et al.*, 2009; Chesi G. *et al.*, 2016). It remains unclear whether isogenic expression of ATP7B-H1069Q equally leads to the fast turnover of the protein. To gain some clarifying insights, we analyzed the expression of ATP7B in HLCs derived from a WD patient and control iPSCs. We compared overall ATP7B quantities in control and patient HLCs using immunofluorescence assay and Western blot analysis. Immunofluorescence analysis revealed that the HLCs derived from patient iPSCs expressed lower levels of ATP7B-H1069Q compared to control HLCs (Fig. 31 A). Likewise, Western blot analysis detected no ATP7B expression in undifferentiated iPSCs from both control and patient HLCs, as well as from unrelated and undifferentiated human iPSCs. In contrast, strong expression was detected in the HLCs derived from the control iPSCs and unrelated human iPSCs (Fig. 31, panel B). Strikingly, the expression level of the mutant protein was rather low, only 30%, compared to control (graph in Fig. 31 B), although ATP7B mRNA levels were similar (data not shown). Furthermore, when HLCs obtained from control and patient iPSCs were incubated in the presence of the protein synthesis inhibitor cycloheximide, a clear reduction in ATP7B-H1069Q was observed after 4 hours in patient HLCs. By contrast, no decrease was seen in the control cells (Fig. 31, panel C). Altogether, these results strongly suggest that endogenously expressed ATP7B-H1069Q accumulates at a steady state at lower levels in patient HLCs because it undergoes a faster degradation than the WT protein.

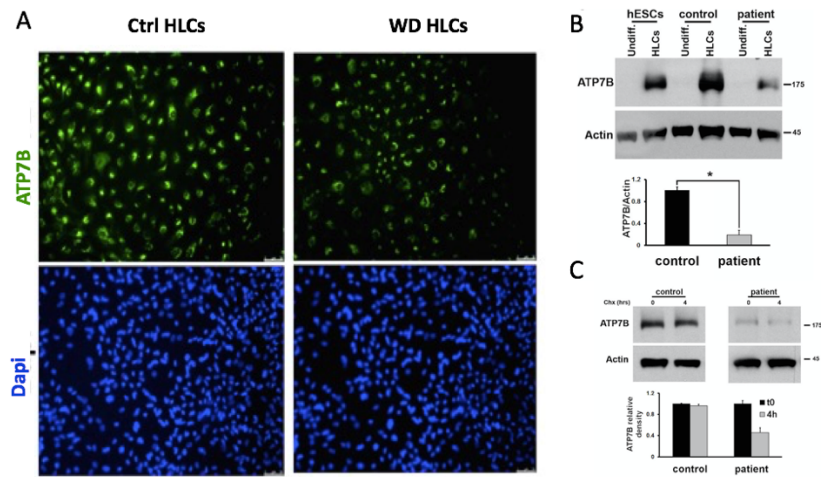


**Figure 31. ATP7B expression in HLCs from patient and control iPSCs.** A. Immunofluorescence analysis of ATP7B expression in HLCs derived from control and patient iPSCs. Nuclei are stained in blue with DAPI. Scale bars: 50  $\mu$ m. B. Representative western blotting of ATP7B accumulation at steady state in undifferentiated iPSCs and in differentiated HLCs. Unrelated human iPSCs were used as further control. Actin was used as loading control. The graph shows the relative expression of ATP7B in patient HLCs normalized to the level in the control HLCs. Data are reported as means  $\pm$  SEM of three biological replicates. C. Western blot analysis of ATP7B accumulation in control and patient HLCs incubated for 4 hours in the absence or in the presence of 100  $\mu$ M Cycloheximide. Actin was used as loading control. The graph shows the relative expression of ATP7B at the 4 hours time point normalized to the level of the 0 time point. Data are reported as means  $\pm$  SEM of three biological replicates.

## 5. CONCLUSIONS AND DISCUSSION

This thesis has presented three main findings. The first is the characterization of CryAB peptide activity on H1069Q mutation of ATP7B, the most frequent cause of WD, in heterologous cells. The second is the generation of an isogenic model system derived from WD patients bearing H1069Q ATP7B mutation to study the properties of endogenously expressed ATP7B-H1069Q. The third is the determination of the effects of phosphorylation on CryAB full length structure and function.

### Characterization of CryAB peptide activity

Currently, whereas about 5% of all WD patients require liver transplantation, less-severely affected patients can benefit from treatment with Cu-chelating agents and zinc. Despite being effective, these treatments cause serious side effects and exhibit limited efficiency in substantial cohorts of patients (Iorio R. *et al.*, 2004; Beinhardt S. *et al.*, 2014). Thus, an alternative therapeutic approach, able to act on ATP7B-H1069Q, the mutated protein causing the great majority of WD cases, would be a great therapeutic breakthrough for WD.

Over the past few years, scientists have identified CryAB-derived peptides that mimic the chaperone activity of the full length protein (mini chaperones). In particular, CryAB-derived peptide corresponding to residues 73-92 has different functions. It acts as a mini-chaperone *in vitro*, protects human lens epithelial cells (HLE) from thermal-stress induced apoptosis, and inhibits selenite-induced cataracts after intraperitoneal injection in rats. Studies indeed suggest that mini-chaperone peptides are potential candidates for therapeutic use in diseases associated with protein aggregation. Remarkably, the beneficial results obtained in rats after receiving intraperitoneal administration of CryAB suggest that this peptide could be used *in vivo* to tackle WD (Nahomi RB. *et al.*, 2013).

Therefore, in the wake of these findings, we decided to investigate the mini-chaperone activity of 73-92 peptide (Pept1) in our WD cellular model. Our results demonstrate that Pept1 enters the cells and does not affect cells viability. Most important, under overload Cu conditions, this peptide works as efficiently as the isolated crystallin domain and full-length CryAB in preventing aggregation and in rescuing ATP7B-H1069Q from the ER to TGN and to the post-TGN trafficking. Furthermore, Pept1 but not the Ctrl

Pept interacts with ATP7B WT and H1069Q, as shown by co-immunoprecipitation assay and FLIM analysis. We also show that Pept1 is able to stabilize ATP7B-H1069Q, thereby increasing its half-life. Looking ahead, all these encouraging results will prompt us to investigate the effect of this CryAB peptide 73-92 on the molecular mechanisms that regulate Cu metabolism in WD pathogenesis.

The use of peptides and peptidomimetics has revolutionary potential in therapy. However, further studies are necessary to develop strategies to optimize mini-chaperone peptides. Many approaches including chemical modifications, D-amino acid and amide bond replacements, cyclization, and novel amino acid substitutions could be used to stabilize and to guarantee better resistance and specificity (Hruby VJ. and Cai M. 2013). Moreover, future studies in animal models are needed to ascertain the toxicity and the delivery of the mini-chaperone to enable its development as a therapeutic agent.

### **Generation of an isogenic ATP7B-H1069Q model system**

Any potential new drug should be first validated in cellular systems closely resembling those of patients, then tested in animal models, and subsequently clinically tried on humans – as clearly shown by the deltaF-CFTR mutant, the most common cause of cystic fibrosis (Peters KW. et al., 2011). Similarly to ATP7B-H1069Q, the deltaF-CFTR mutant is extensively retained in the ER. Over the years, many screening libraries have identified both molecular targets and chemical compounds to efficiently correct CFTR (Lukacs GL. and Verkman AS. 2012). However, most of the correction strategies have failed to rescue CFTR function in patient-derived cells. The main cause of this failure is that these correction strategies are performed by overexpressing the mutant protein in heterologous cells. Thus, the only reliable option for *in vitro* validation of novel correction disease-relevant cellular systems is to exploit the isogenic expression of the pathogenic mutant. Unfortunately, any similar cellular system remains unavailable for ATP7B-H1069Q. Despite the rapid development of gene editing technologies, neither hepatic cell lines nor vertebrate animal models with endogenous expression of ATP7B-H1069Q mutant have been generated. One possible solution to tackle this problem would be to obtain hepatocytes from patients' liver biopsies. However, owing to the scant number of cells in a biopsy and the inability of hepatic cells to proliferate *in vitro*, drug validation would be nearly impossible. For this reason, nowadays skin fibroblasts are being widely used to validate

drugs in a number of diseases – the reason being that these cells can easily be obtained by patients and expand *in vitro* (Huch M. and Koo BK, 2015). In this context, in collaboration with Dr. Silvia Parisi, Anna Musto, Simona Allocca, and Roman Polishchuk, we generated a novel cell model to study the H1069Q mutation of ATP7B. This model is based on the generation of iPSCs obtained by reprogramming primary skin fibroblasts from a homozygous patient and from his mother, used as control, and by subsequently differentiating them into HLCs. Remarkably, we found that endogenously expressed ATP7B-H1069Q accumulates at a lower steady state level in patient HLCs because it undergoes a faster degradation than the WT protein.

The availability of this model has thus become paramount. Actually, several studies have previously reported on the generation of iPSCs from WD patient with R778L and M769V genetic mutations of ATP7B (Zhang S. *et al.*, 2011; Yi F. *et al.*, 2012), but not with the ATP7B-H1069Q mutant. Therefore, the novelty of our research lies in the generation of human iPSCs from a patient bearing the H1069Q-ATP7B mutation.

Noteably, another major advantage of our approach is that of having used a family member as control (the patient's mother) as opposed to previous works which have used human ESCs derived from human embryo of unrelated individuals. Moreover, as 40-50% of WD patients (Walshe JM, 1962) develop neurological defects, this approach will also allow us to differentiate patient-derived iPSCs into neurons to better study the effect of H1069Q mutation on brain dysfunction.

Thus, we are confident that this disease-relevant system with the isogenic expression of H1069Q mutation of ATP7B represents a novel model for *in vitro* validation of novel correction strategies in WD.

### **Effects of phosphorylation on CryAB chaperone activity**

Protein phosphorylation is the major post-translational modification in eukaryotic cells. This post-translational modification plays a crucial role in the cellular functions of proteins such as sHSP, particularly CryAB (Katsogiannou M. *et al.*, 2014). Recent findings demonstrate that phosphorylation of CryAB at serine residues interferes with its chaperone activity and oligomerization. In particular, pseudo-phosphorylated CryAB-S19D and -S45D have an inhibitory effect, either alone or in combination. By contrast -S59D has no such effect and counteracts the inhibition caused by single phosphomimetic substitutions at S19 and S45. Interestingly, all phosphomimetic substitutions lead to significantly decreased oligomeric

size of the protein, indicating that the inhibitory effect seen for S19 and S45 cannot be ascribed to the reduction of oligomerization.

Although several reports have investigated the effects of phosphorylation on the chaperone activity and oligomerization of CryAB, the results are controversial. For instance, recent work has demonstrated that mimicking phosphorylation only on Ser-59 protects cardiac myocytes against apoptosis by conferring maximal cytoprotection. A possible explanation to this phenomenon is that CryAB confers cytoprotection by interacting with many targets in addition to caspase-3. CryAB monomers associate with each other forming oligomers. The mass of the oligomers decreases in response to cellular stresses that, in turn, increase CryAB phosphorylation (Muchowski P.J. *et al.*, 1999; Ito H. *et al.*, 2001; Chiesi M. *et al.*, 1990), suggesting that the phosphorylated CryAB monomers translocate to sites where they mediate cytoprotection. These results also imply that CryAB monomers serve as efficient chaperones (Morrison LE. *et al.*, 2015). In glioma cells, using centrifugation on a sucrose density gradient, researchers show that pseudophosphorylation at the serine residues 19, 45, 59 determines the formation of small oligomers associated with a reduced chaperone activity (Ito H. *et al.*, 2001). By contrast R120G mutation, which is known to cause desmin-related cardiomyopathy, forms great oligomers (over 645 kDa); yet, this form is defective in chaperone activity (Bova MP. *et al.*, 1999). Thus, phosphorylation status, CryAB oligomerization state, and chaperone activity have no direct and simple relationships. Most likely, CryAb is endowed with a fine regulatory system that recognizes different client proteins where phosphorylation plays an important role in controlling this activity. This line of research clearly warrants further investigation.

Regarding a possible explanation for how phosphorylation controls CryAB chaperone activity, studies show that CryAB uses its intrinsic structural plasticity to expose distinct binding interfaces and thus interacts with a wide range of structurally variable clients (Mainz A. *et al.*, 2015). This observation led us to speculate that phosphorylation plays an important role in controlling CryAB conformation state and plasticity. Consequently, any change in phosphorylation patterns may differently interfere with CryAB chaperone function. For instance, studies show that the phosphorylation pattern that inhibits chaperone activity of CryAB for FZ4-FEVR and ATP7B-H1069Q (S19D, S45D, S19 /45D or 3D) better protects k-casein but not the formation of amyloid fibers c $\beta$ -Trp peptide (Ecroyd H. *et al.*, 2007). Thus, CryAB phosphorylation has a different effect depending on the aggregation prone protein engaged.

It has been recently reported that MAPK signaling pathways have a crucial role in the response to endoplasmic reticulum stress and unfolded protein

response (UPR) (Darling N.J. *et al.*, 2014). In particular, the MAPK signaling pathway is essential in regulating many cellular processes including cell cycle progression, cell survival, apoptosis, inflammation, cell stress response, and cell differentiation. (Pimienta G. and Pascual J., 2007; Raman M. *et al.*, 2007; Shaul Y.D. *et al.*, 2007). Among conventional MAPKs (ERK1/2, JNK and p38), ERK1/2 and p38 seem to have a fundamental role in the regulation of several HSPs including CryAB (Robitaille H. *et al.*, 2010; Mitra A. *et al.*, 2014; Zhu Z. *et al.*, 2015). In particular, whereas S45 (and possibly S19) is phosphorylated by ERK1/2, S59 is phosphorylated by p38-dependent MAPK (Kato K. *et al.*, 1998). Most important, p38 MAPK down-regulates ERK1/2 (Lu Z. *et al.*, 2006), suggesting that in the cell, phosphorylation on serine residue 59 may be followed by a negative regulation of the phosphorylation at serine residues 19 and 45. Thus, the protective role of phosphomimetic S59 when CryAB is also pseudophosphorylated on serine 19 or 45 is accompanied by the negative regulation of ERK1/2 by p38 MAPK. Interestingly, recent findings have shown that ATP7B-H1069Q overexpression in HepG2 cells activates p38 MAPK, which, in turn, favors its retention in the ER and rapid degradation. By contrast, suppression of this pathway by p38 inhibitors results in substantial rescue of ATP7B-H1069Q from the ER to TGN compartment (Chesi G. *et al.*, 2016). However, as CryAB is expressed at very low levels in hepatocytes and hepatoma cell lines, these observations should be verified in cell expressing significant amount of the chaperone.

Conversely, p38 kinase activity is required for the phosphorylation-dependent nuclear translocation of the spliced form of the X-box binding protein 1 (Xbp1s). Perturbations of ER homeostasis can create an ER stress and determine the activation of a group of complex signaling pathways known as unfolded protein response (UPR). Xbp1s is produced during UPR, which normally occurs when unfolded proteins accumulate in the ER. (Lee J. *et al.*, 2011). Since TMPs exhibit domains on both the luminal and the cytosolic side of the ER, mutations affecting their folding and export from the ER most likely require the coordinated activation of chaperones acting from both sides of the ER membrane. Accordingly, the MAPK signaling pathway could provide this coordination by participating in UPR both to generate the response in the lumen and, simultaneously to protect CryAB cytosolic chaperone activity to assist TMPs (Ciano M. *et al.*, 2016).

## **6. ACKNOWLEDGEMENTS**

This work was supported by Telethon grant n. GGP 14002 to S.B. I wish to thank Prof. Massimo Mallardo and Dr. Maria Gabriella Caporaso for their technical help and useful advises and Dr. Paola Merolla for editing the final draft of my thesis.

## 7. REFERENCES

**Allocca Simona Ph.D thesis.** New Therapeutic Perspectives for the Most Frequent ATP7B Mutation in Wilson Disease: Development of Pharmacologically Active Peptides and Generation of a Novel WD Isogenic Cell Model.

**Adhikari AS, Singh BN, Rao KS, Rao ChM.**  $\alpha$ B-crystallin, a small heat shock protein, modulates NF- $\kappa$ B activity in a phosphorylation-dependent manner and protects muscle myoblasts from TNF- $\alpha$  induced cytotoxicity. *Biochim Biophys Acta.* (2011); 1813:1532-1542.

**Aquilina J.A, Benesch J.L, Ding L.L, Yaron O, Horwitz J, Robinson C.V.** Phosphorylation of alphaB-crystallin alters chaperone function through loss of dimeric substructure. *J. Biol. Chem.* (2004); 279, 28675-28680.

**Arredondo M, Núñez MT.** Iron and copper metabolism. *Mol Aspects Med.* (2005); 26(4-5): 313-27.

**Arrigo A. P, Simon S, Gibert B, Kretz-Remy C, Nivon M., Czekalla A, Guillet, D, Moulin M., Diaz-Latoud C. and Vicart P.** Hsp27 (HspB1) and alphaB-crystallin (HspB5) as therapeutic targets. *FEBS Lett.* (2007); 581, 3665-3674.

**Asomugha CO, Gupta R, Srivastava OP.** Structural and functional roles of deamidation of N146 and/or truncation of NH2- or COOH-termini in human B-crystallin. *Mol Vis.* (2011); 17:2407-2420.

**Banci L, Bertini I, Cantini F, Rosenzweig A and Yatsunyk LA.** Metal binding domains 3 and 4 of the Wilson disease protein: Solution structure and interaction with the copper (I) chaperone HAH1. *Biochemistry.* (2008); 47: 7423-7429.

**Bakthisaran R, Akula K.K, Tangirala R, Rao Ch M.** Phosphorylation of alphaBcrystallin: role in stress, aging and patho-physiological conditions, *Biochim. Biophys. Acta.* (2016); 1860: 167-182.

**Beinhardt S, Leiss W, Stättermayer AF, Graziadei I, Zoller H, Stauber R, Maieron A, Datz C, Steindl-Munda P, Hofer H, Vogel W, Trauner**

**M, Ferenci P.** Long-term outcomes of patients with Wilson disease in a large Austrian cohort. *Clin Gastroenterol Hepatol.* (2014); 12(4):683-9.

**Bhattacharyya J, Udupa EGP, Wang J, Sharma KK.** Mini- $\alpha$ B-crystallin: a functional element of  $\alpha$ B-crystallin with chaperone-like activity. *Biochemistry.* (2006); 45, 3069-76.

**Bloemendal H, de Jong W, Jaenicke R, Lubsen NH, Slingsby C, Tardieu A.** Ageing and vision: structure, stability and function of lens crystallins. *Prog Biophys Mol Biol.* (2004); 86:407-85.

**Bloemendal H.** The lens proteins. In: Bloemendal H, editor. *Molecular and Cellular Biology of the Eye Lens.* New York: John Willey & Sons; (1981). pp. 1-49.

**Boelens WC, Croes Y, de Jong WW.** Interaction between alphaB-crystallin and the human 20S proteasomal subunit C8/alpha7. *Biochim Biophys Acta.* (2001); 1544:311-319.

**Bova MP, Yaron O, Huang Q, Ding L, Haley DA, Stewart PL and Horwitz J.** Mutation R120G in alphaB-crystallin, which is linked to a desmin-related myopathy, results in an irregular structure and defective chaperone-like function. *Proc Natl Acad Sci USA.* (1999); 96:6137-6142.

**Bartelt-Kirbach B. and Golenhofen N.** Reaction of small heat-shock proteins to different kinds of cellular stress in cultured rat hippocampal neurons. *Cell Stress Chaperones.* (2014); 19(1):145-53.

**Cater M.A, Forbes J, La Fontaine S, Cox D, Mercer FJ.** Intracellular trafficking of the human Wilson protein: the role of the six N-terminal metal-binding sites. *Biochem J.* (2004); 380(Pt3): 805-13.

**Cater M. A, La Fontaine S, Shield K, Deal Y. and Mercer J. F.** ATP7B mediates vesicular sequestration of copper: insight into biliary copper excretion. *Gastroenterology.* (2006); 130, 493-506.

**Chandhok G, Schmitt N, Sauer V, Aggarwal A, Bhatt M, Schmidt HH.** The Effect of Zinc and D-Penicillamine in a Stable Human Hepatoma ATP7B Knockout Cell Line. *PLoS One.* (2014); 9(6): e98809.

**Chandhok G, Horvath J, Aggarwal A, Bhatt M, Zibert A and Schmidt.** Functional analysis and drug response to zinc and D-penicillamine in stable ATP7B mutant hepatic cell lines. *World J Gastroenterol.* (2016); 22(16): 4109-4119.

**Chesi G, Hegde R.N, Iacobacci S, Concilli M, Parashuraman S, Festa B.P, Polishchuk E.V, Di Tullio G, Carissimo A, Montefusco S, Canetti D, Monti M, Amoresano A, Pucci P, van de Sluis B, Lutsenko S, Luini A, Polishchuk R.S.** Identification of p38 MAPK and JNK as new targets for correction of Wilson disease-causing ATP7B mutants. *Hepatology.* (2016); 63: 1842-1859.

**Chiesi M, Longoni S, Limbruno MU.** Cardiac  $\alpha$ -crystallin, III: involvement during heart ischemia. *Mol Cell Biochem.* (1990); 97:129-136.

**Ciano M, Allocca S, Ciardulli M. C, della Volpe L, S. Bonatti, D'Agostino M.** Differential phosphorylation-based regulation of  $\alpha$ Bcrystallin chaperone activity for multipass transmembrane proteins. *Biochemical and Biophysical Research Communications.* (2016); 479(2): 325-330.

**Concilli M, Iacobacci S, Chesi G, Carissimo A, Polishchuk R.** A systems biology approach reveals new endoplasmic reticulum-associated targets for the correction of the ATP7B mutant causing Wilson disease. *Metallomics.* (2016); 8 (9), 920-930.

**D'Agostino M, Lemma V, Chesi G, Stornaiuolo M, Cannata Serio M, D'Ambrosio C, Scaloni A, Polishchuk R and Bonatti S.** The cytosolic chaperone  $\alpha$ -Crystallin B rescues appropriate folding and compartmentalization of misfolded multispan transmembrane proteins. *J Cell Sci.* (2013); 126:4160-4172.

**de Bie P, Muller P, Wijmenga C, Klomp LW.** Molecular pathogenesis of Wilson and Menkes disease: correlation of mutations with molecular defects and disease phenotypes. *J Med Genet.* (2007); 44:673-688.

**Darling N.J, Cook S.J.** The role of MAPK signalling pathways in the response to endoplasmic reticulum stress, *Biochim. Biophys. Acta.* (2014); 1843: 2150-2163.

**Di Donato M, Hsu HF, Narindrasorasak S, Que L Jr, Sarkar B.** Copper-induced conformational changes in the N-terminal domain of the Wilson disease copper-transporting ATPase. *Biochemistry*. (2000); 39; 1890-1896.

**Di Donato M, Zhang J, Que L Jr, Sarkar B.** Zinc binding to the NH<sub>2</sub>-terminal domain of the Wilson disease copper-transporting ATPase: implications for in vivo metal ion-mediated regulation of ATPase activity. *J Biol Chem*. (2002); 277; 13409-13414.

**Dmitriev OY, Bhattacharjee A, Nokhrin S, Uhlemann E-ME and Lutsenko S.** Difference in stability of the N-domain underlies distinct intracellular properties of the E1064A and H1069Q mutants of copper-transporting protein ATPase ATP7B. *J Biol Chem*. (2011); 286: 16355-16362.

**Ecroyd H, Meehan S, Horwitz J, Aquilina J.A, Benesch J.L, Robinson C.V, Macphee C.E, Carver J.A.** Mimicking phosphorylation of alphaB-crystallin affects its chaperone activity, *Biochem. J*. (2007); 401: 129-141.

**Efremov RG, Kosinsky YA, Nolde DE, Tsivkovskii R, Arseniev AS, Lutsenko S.** Molecular modelling of the nucleotide-binding domain of Wilson's disease protein: location of the ATP-binding site, domain dynamics and potential effects of the major disease mutations. *Biochem J*. (2004); 382; 293-305.

**Ferenci P.** Review article: diagnosis and current therapy of Wilson's disease. *Aliment Pharmacol Ther*. (2004); 19: 157-165.

**Ghosh JG. And Clark JI.** Insight into the domains required for dimerization and assembly of human alphaB crystalline. *Protein Sci*. (2005). 14(3): 684-695.

**Ghosh JG, Houck SA and Clark JI.** Interactive sequences in the molecular chaperone, human alphaB crystalline modulate the fibrillation of amyloidogenic proteins. *Int J Biochem cell Biol*. (2008); 40: 954-967.

**Ghosh JG, Shenoy AK, Jr, Clark JI.** Interactions between important regulatory proteins and human alphaB crystallin. *Biochemistry*. (2007a); 46: 6308-6317.

**Gitlin JD.** Wilson disease. *Gastroenterology*. (2003); 125: 1868-1877.

**Gromadzka G, Schmidt H.H, Genschel J, Bochow B, Rodo M, Tarnacka B, Litwin T, Chabik G, Czonkowska.** A Frameshift and non sense mutations in the gene for ATPase are associated with sever impairment of copper metabolism and with an early clinical manifestation of Wilson's disease. *Clin.Genet*. (2005); 68, 524-532.

**Gupta R, Srivastava OP.** Deamidation affects structural and functional properties of human alphaA-crystallin and its oligomerization with alphaB-crystallin. *J Biol Chem*. (2004); 279: 44258-44269.

**Haslbeck M, and Buchner J.** Chaperone function of sHsps. *Prog Mol Subcell Biol*. (2002); 28: 37-59.

**Horwitz J.**  $\alpha$ -Crystallin can function as a molecular chaperone. *Proc Natl Acad Sci USA*. (1992); 89, 10449-53.

**Hruby VJ and Cai M.** Design of Peptide and Peptidomimetic Ligands with Novel Pharmacological Activity Profiles. *Ann Rev Pharmacol Toxicol*. (2013); 53, 557-580.

**Hsi G, Cullen LM, Moira Glerum D, Cox DW.** Functional assessment of the carboxy-terminus of the Wilson disease copper-transporting ATPase, ATP7B. *Genomics*. (2004); 83; 473-481.

**Huch M, Koo BK.** Modeling mouse and human development using organoid cultures. *Development*. (2015); 142(18):3113-25.

**Huster D, Hoppert M, Lutsenko S, Zinke J, Lehmann C, Mossner J, Berr F, Caca K.** Defective cellular localization of mutant ATP7B in Wilson's disease patients and hepatoma cell lines. *Gastroenterology*. (2003); 124; 335-45.

**Huster D, Kühne A, Bhattacharjee A, Raines L, Jantsch V, Noe J, Schirrmeister W, Sommerer I, Sabri O, Berr F, Mössner J, Stieger B, Caca K, Lutsenko S.** Diverse Functional Properties of Wilson Disease ATP7B Variants. *Gastroenterology*. (2012); 142(4): 947-956.

**Iida M, Terada K, Sambongi Y, Wakabayashi T, Miura N, Koyama K, Futai M.** Analysis of functional domains of Wilson disease protein (ATP7B) in *Saccharomyces cerevisiae*. *FEBS Lett*. (1998); 428: 281-285.

**Iorio R, D'Ambrosi M, Marcellini M, Barbera C, Maggiore G, Zancan L, Giacchino R, Vajro P, Marazzi MG, Francavilla R, Michielutti F, Resti M, Frediani T, Pastore M, Mazzarella G, Fusco G, Cirillo F, Vegnente A; Hepatology Committee of Italian Society of Paediatric Gastroenterology Hepatology and Nutrition.** Serum transaminases in children with Wilson's disease. *J Pediatr Gastroenterol Nutr.* (2004); 39(4): 331-6.

**Ito H, Okamoto K, Nakayama H, Isobe T, Kato K.** Phosphorylation of  $\alpha$ B-crystallin in response to various types of stress. *J Biol Chem.* (1997); 272: 29934-29941.

**Ito H, Kamei K, Iwamoto I, Inaguma Y, Nohara D, Kato K.** Phosphorylation-induced change of the oligomerization state of alpha B-crystallin. *J Biol Chem.* (2001); 276, 5346-5352.

**Kaler SG.** ATP7A-related copper transport diseases-emerging concepts and future trends. *Nat Rev Neurol.* (2011); 7: 15-29.

**Kannan R, Sreekumar PG and Hinton DR.** Novel roles for alpha-crystallins in retinal function and disease. *Prog Retin Eye Res.* (2012); 31: 56-604.

**Kato K, Ito H, Kamei K, Inaguma Y, Iwamoto I, Saga S.** Phosphorylation of  $\alpha$ B-crystallin in mitotic cells and identification of enzymatic activities responsible for phosphorylation. *J Biol Chem.* (1998); 273: 28346-28354.

**Katsogiannou M, Andrieu C, Rocchi P.** Heat shock protein 27 phosphorylation state is associated with cancer progression. *Front. Genet.* (2014); 5:346.

**Kodama H, Murata Y, Kobayashi M.** Clinical manifestations and treatment of Menkes disease and its variants. *Pediatr Int.* (1999); 41, 423-429.

**Launay N, Tarze A, Vicart P, Lilienbaum A.** Serine 59 phosphorylation of  $\alpha$ B-crystallin down-regulates its anti-apoptotic function by binding and sequestering Bcl-2 in breast cancer cells. *J Biol Chem.* (2010); 285 (48): 37324-32.

- Lee J, Sun C, Zhou Y, Lee J, Gokalp D, Herrema H, Park S.W, Davis R. J, Ozcan U.** p38 MAPK-mediated regulation of Xbp1s is crucial for glucose homeostasis. *Nat. Med.* (2011); 17: 1251-1260.
- Lukacs GL, Verkman AS.** CFTR: folding, misfolding and correcting the  $\Delta F508$  conformational defect. *Trends Mol Med.* (2012); 18(2): 81-91.
- Lu Z, Xu S.** ERK1/2 MAP kinases in cell survival and apoptosis, *IUBMB Life.* (2006); 58: 621-631.
- Lutsenko S, Barnes NL, Bartee MY, Dmitriev OY.** Function and regulation of human copper transporting ATPases. *Physiol Rev.* (2007); 87: 1011-1046.
- Lutsenko, S.** Human copper homeostasis: a network of interconnected pathways. *Curr. Opin. Chem. Biol.* (2010); 14, 211–217.
- Mainz A, Peschek J, Stavropoulou M, Back K.C, Bardiaux B, Asami S, Prade E, Peters C, Weinkauff S, Buchner J, Reif B.** The chaperone  $\alpha$ Bcrystallin uses different interfaces to capture an amorphous and an amyloid client. *Nat. Struct. Mol. Biol.* (2015); 22: 898-905.
- Mercer JF, Barnes N, Stevenson J, Strausak D, Llanos RM.** Copper-induced trafficking of the Cu-ATPases: a key mechanism for copper homeostasis. *Biometals.* (2003); 16; 175-184.
- Miller J.V, Juul B, Maire M.** Structural organization, ion transport, and energy transduction of P-type ATPases. *Biochim. Biophys. Acta.* (1996); 1286, 1-51.
- Mitra A, Ray A, Datta R, Sengupta S, Sarkar S.** Cardioprotective role of P38 MAPK during myocardial infarction via parallel activation of  $\alpha$ -crystallin B and Nrf2. *J. Cell Physiol.* (2014); 1272-1282.
- Morrison L.E, Hoover H.E, Thuerauf D. J, Glembotski C. C.** Mimicking phosphorylation of  $\alpha$ -B-Crystallin on Serine-59 Is Necessary and Sufficient to Provide Maximal Protection of Cardiac Myocytes From Apoptosis. *Circulation Research.* (2003); 92(2): 203-11.
- Muchowski PJ, Wu GJ, Liang JJ, Adman ET, Clark JI.** Site-directed mutations within the core “ $\alpha$ -crystallin” domain of the small heat-shock

protein, human  $\alpha$ -B-crystallin, decrease molecular chaperone functions. *J Mol Biol.* (1999); 289: 397-411.

**Nagaraj RH, Oya-Ito T, Padayatti PS, Kumar R, Mehta S, West K, Levison B, Sun J, Crabb JW, Padival AK.** Enhancement of chaperone function of  $\alpha$ -crystallin by methylglyoxal modification. *Biochemistry.* (2003); 42: 10746-10755.

**Nagaraj RH, Hahomi R.B, Mueller N.H., Raghavan C.T, Ammar J, Petrash M.** Therapeutic potential of  $\alpha$ -crystallin. *Biochimica et Biophysica Acta.* (2015); 1860 (100): 252-257.

**Nahomi RB, Wang B, Raghavan CT, Voss O, Doseff AI, Santhoshkumar P, Nagaraj RH.** Chaperone peptides of  $\alpha$ -crystallin inhibit epithelial cell apoptosis, protein insolubilization, and opacification in experimental cataracts. *J Biol Chem.* (2013); 288(18): 13022-35.

**Nahomi RB, DiMauro MA, Wang B, Nagaraj RH.** Identification of peptides in human Hsp20 and Hsp27 that possess molecular chaperone and anti-apoptotic activities. *Biochem J.* (2015); 465(1): 115–125.

**Narberhaus F.**  $\alpha$ -Crystallin-type heat shock proteins: socializing minichaperones in the context of a multichaperone network. *Microbiol Mol Biol Rev.* (2002); 66, 64-93.

**Nevitt T, Ohrvik H, and Thiele D.J.** Charting the travels of copper in eukaryotes from yeast to mammals. *Biochim. Biophys. Acta.* (2012); 1823, 1580-1593.

**Okita K, Matsumura Y, Sato Y, Okada A, Morizane A, Okamoto S, Hong H, Nakagawa M, Tanabe K, Tezuka K, Shibata T, Kunisada T, Takahashi M, Takahashi J, Saji H, Yamanaka S.** A more efficient method to generate integration-free human iPS cells. *Nat Methods.* (2011); 8(5): 409-12.

**Payne AS, Kelly EJ, Gitlin JD.** Functional expression of the Wilson disease protein reveals mislocalization and impaired copper-dependent trafficking of the common H1069Q mutation. *Proc Natl Acad Sci U S A* (1998); 95:10854-10859.

**Peters KW, Okiyoneda T, Balch WE, Braakman I, Brodsky JL,**

**Guggino WB, Penland CM, Pollard HB, Sorscher EJ, Skach WR et al.** CFTR Folding Consortium: methods available for studies of CFTR folding and correction. *Methods Mol Biol.* (2011); 742: 335-353.

**Petris MJ, Camakaris J, Greenough M, LaFontaine S, Mercer JF.** A C-terminal di-leucine is required for localization of the Menkes protein in the trans-Golgi network. *Hum Mol Genet.* (1998); 7: 2063– 2071.

**Petris M.J, Voskoboinik I, Cater M, Smith K, Kim B.E, Llanos R.M, Strausak D, Camakaris J, Mercer J.F.B.** Copper-regulated trafficking of the Menkes disease copper ATPase is associated with formation of a phosphorylated catalytic intermediate. *J. Biol. Chem.* (2002); 277, 46736-46742.

**Pimienta G, Pascual J.** Canonical and alternative MAPK signaling, *Cell Cycle.* (2007); 2628-2632.

**Plater M.L, Goode D. and Crabbe M.J.C.** Effects of site-directed mutations on the chaperone-like activity of  $\alpha$ B-crystallin. *JBC.* (1996); 271, 28558-28566.

**Porteus MH and Carroll D** Gene targeting using zinc finger nucleases. *Nat Biotechnol.* (2005); 23: 967-973.

**Qian Y, Zheng Y, Ramos KS, Tiffany-Castiglioni E.** The involvement of copper transporter in lead-induced oxidative stress in astroglia. *Neurochem Res.* (2005); 30; 429-438.

**Rajagopal P, Tse E, Borst A.J., Delbecq S.P, Shi L, Southworth D.R, Klevit R.E.** A conserved histidine modulates HSPB5 structure to trigger chaperone activity in response to stress related acidosis. *eLife.* (2015); 4: e07304.

**Raju M, Santhoshkumar P, Krishna Sharma K.** Alpha-crystallin-derived peptides as therapeutic chaperones. *Biochim Biophys Acta.* (2016); 1860, 246-5.

**Raman M, Chen W, Cobb M.H.** Differential regulation and properties of MAPKs. *Oncogene.* (2007); 26: 3100-3112.

**Roberts E.A, Schilsky M.L; Division of Gastroenterology and Nutrition, Hospital for Sick Children, Toronto, Ontario, Canada.** A practice guideline on Wilson disease. *Hepatology*. (2003); 37(6): 1475-92.

**Roberts E.A. and Schilsky M.L.** Diagnosis and treatment of Wilson disease: an update. *Hepatology*. (2008); 47, 2089-111.

**Robitaille J, MacDonald M.L, Kaykas A, Sheldahl L.C, Zeisler J, Dube M.P, Zhang L.H, Singaraja R.R, Guernsey D.L, Zheng B, Siebert L.F., Hoskin-Mott A, Trese M.T, Pimstone S.N, Shastry B.S, Moon R.T, Hayden M.R, Goldberg Y.P, Samuels M.E.** Mutant frizzled-4 disrupts retinal angiogenesis in familial exudative vitreoretinopathy, *Nat. Genet*. (2002); 32: 326-330.

**Robitaille H, Simard-Bisson C, Larouche D, Tanguay R.M, Blouin R, Germain L.** The small heat-shock protein Hsp27 undergoes ERK-dependent phosphorylation and redistribution to the cytoskeleton in response to dual leucine zipper-bearing kinase expression, *J. Investig. Dermatol*. (2010); 130: 74-85.

**Schwarz L, Vollmer G, and Richter-Landsberg C.** The Small Heat Shock Protein HSP25/27 (HspB1) Is Abundant in Cultured Astrocytes and Associated with Astrocytic Pathology in Progressive Supranuclear Palsy and Corticobasal Degeneration. *International Journal of Cell Biology*. (2010); ID 717520, 10 pages.

**Sharma KK, Kaur H. Kathryn K.** Functional elements in molecular chaperone  $\alpha$ -crystallin: identification of binding sites in  $\alpha$ B-crystallin. *Biochemical and Biophysical Research Communications*. (1997); 239:(1) 217-222.

**Sharma KK, Kumar RS, Kumar GS, Quinn PT.** Synthesis and characterization of a peptide identified as a functional element in  $\alpha$ A-crystallin. *J Biol Chem*. (2000); 275, 3767-71.

**Shaul Y.D, Seger R.** The MEK/ERK cascade: from signaling specificity to diverse functions, *Biochim. Biophys. Acta*. (2007); 1773: 1213-1226.

**Si-Tayeb K, Noto FK, Nagaoka M, Li J, Battle MA, Duris C, North PE, Dalton S, Duncan SA.** Highly efficient generation of human hepatocyte-like cells from induced pluripotent stem cells. *Hepatology*. (2010); 51(1):

297-305.

**Song MO, Freedman JH.** Expression of copper-responsive genes in HepG2 cells. *Mol Cell Biochem.* (2005); 279: 141–147.

**Sreekumar PG, Chothe P, Sharma KK, Baid R, Kompella U, Spee C, Kannan N, Manh C, Ryan SJ, Ganapathy V, Kannan R and Hinton DR.** Antiapoptotic Properties of  $\alpha$ -Crystallin-Derived Peptide Chaperones and Characterization of Their Uptake Transporters in Human RPE Cells. *Invest Ophthalmol Vis Sci* (2013); 54: 2787-2798.

**Takeuchi N, Ouchida A, Kamei A.** C-terminal truncation of alpha-crystallin in hereditary cataractous rat lens. *Biol Pharm Bull.* (2004); 27: 308-314.

**Thampi P, Hassan A, Smith JB, Abraham EC.** Enhanced C-terminal truncation of alphaA- and alphaB-crystallins in diabetic lenses. *Invest Ophthalmol Vis Sci.* (2002); 43: 3265-3272.

**Thomas G. R, Forbes J. R, Roberts E. A, Walshe J. M, Cox D. W.** The Wilson disease gene: spectrum of mutations and their consequences. *Nat. Genet.* (1995); 9: 210-217.

**Treweek T.M, Rekas A, Lindner R.A, Walker M.J, Aquilina J.A, Robinson C.V, Horwitz J, Perng M.D, Quinlan R.A, Carver J.A.** R120G alphaB-crystallin promotes the unfolding of reduced alpha-lactalbumin and is inherently unstable, *FEBS J.* (2005); 272, 711-724.

**van den Berghe PV, Stapelbroek JM, Krieger E, de Bie P, van de Graaf SF, de Groot RE, van Beurden E, Spijker E, Houwen RH, Berger R, Klomp LW.** Reduced expression of ATP7B affected by Wilson disease-causing mutations is rescued by pharmacological folding chaperones 4-phenylbutyrate and curcumin. *Hepatology* (2009); 50: 1783-1795.

**van den Berghe P.V, Folmer D, Malingré H. E., van Beurden, E, Klomp A. E, van de Sluis B, Merckx M, Berger R. and Klomp L. W.** Human copper transporter 2 is localized in late endosomes and lysosomes and facilitates cellular copper uptake. *Biochem. J.* (2007); 407, 49-59.

**Vicart P, Caron A, Guicheney P, Lil Z, Prévost M.C, Faure A, Château D, Chapon F, Tomé F, Dupret J.M, Paulin D, Fardeau M.** A missense

mutation in the  $\alpha$ B-crystallin chaperone gene causes a desmin-related myopathy. *Nature Genetics*. (1998); 20, 92-5.

**Yi F, Qu J, Li M, Suzuki K, Kim NY, Liu GH, Belmonte JC.** Establishment of hepatic and neural differentiation platforms of Wilson's disease specific induced pluripotent stem cells. *Protein Cell*. (2012); (11): 855-63.

**Walshe JM.** Wilson's disease. The presenting symptoms. *Arch Dis Child*. (1962) 37:265-6.

**Wu F, Wang J, Pu C, Qiao L, Jiang C.** Wilson's Disease: A Comprehensive Review of the Molecular Mechanisms. *Int. J. Sci.* (2015); 16, 6419-6431.

**Zhang S, Chen S, Li W, Guo X, Zhao P, Xu J, Chen Y, Pan Q, Liu X, Zychlinski D, Lu H, Tortorella MD, Schambach A, Wang Y, Pei D, Esteban MA.** Rescue of ATP7B function in hepatocyte-like cells from Wilson's disease induced pluripotent stem cells using gene therapy or the chaperone drug curcumin. *Hum Mol Genet*. (2011) 20(16): 3176-87.

**Zhang X, Dudek EJ, Liu B, Ding L, Fernandes AF, Liang JJ, Horwitz J, Taylor A, Shang F.** Degradation of C-terminal truncated alpha A-crystallins by the ubiquitin-proteasome pathway. *Invest Ophthalmol Vis Sci*. (2007); 48:4200-4208.

**Zhu Z, Li R, Stricker R, Reiser G.** Extracellular alpha-crystallin protects astrocytes from cell death through activation of MAPK, PI3K/Akt signaling pathway and blockade of ROS release from mitochondria, *Brain Res*. (2015);1620: 17-28.

## 8. LIST OF PUBLICATIONS

**Massi D, Brusa D, Merelli B, Ciano M, Audrito V, Serra S, Buonincontri R, Baroni G, Nassini R, Minocci D, Cattaneo L, Tamborini E, Carobbio A, Rulli E, Deaglio S, Mandalà M.** PD-L1 marks a subset of melanomas with a shorter overall survival and distinct genetic and morphological characteristics. *Annals of oncology*; 25(12): 2433-42. December 2014. PMID: 25223485. ISSN:15698041

**Di Caprio R, Ciano M, Montano G, Costanzo P, Cesaro E.** KAP1 is a novel substrate for the arginine methyltransferase PRMT5 *Biology*; 4(1): 41-49. March 2015. PMCID: PMC4381216. ISSN:2079-7737.

**Ciano M\***, Allocca S\*, Ciardulli M. C, della Volpe L, Bonatti S, D'Agostino M. Differential phosphorylation-based regulation of aBcrystallin chaperone activity for multipass transmembrane proteins. *Biochemical and Biophysical Research Communications*. 479(2): 325-330. October 2016. PMCID: PMC5053547, ISSN:10902104

\* These authors contributed equally to this work

**Busiello T\***, **Ciano M\***, Romano S, Sodaro G, Garofalo O, Bruzzese D, Simeone L, Chiurazzi F, Romano F, Costanzo P, Cesaro E. Role of ZNF224 in cell growth and chemoresistance of chronic lymphocytic leukemia. *Human Molecular Genetics*. Volume 26, Issue 2, January 2017, Pages 344-353. PMID 28040726, ISSN: 14602083.

\* These authors contributed equally to this work

Manuscript submitted:

**Parisi S, Polishchuk E. V, Allocca S, Ciano M, Musto A, Gallo M, Perone L, Ranucci G, Iorio R, Polishchuk R. S, Bonatti S.** Characterization of the most frequent ATP7B mutation causing Wilson disease in hepatocytes derived from patient induced pluripotent stem cells.